



**HAL**  
open science

# Hydrological Signals in Height and Gravity in Northeastern Italy inferred from Principal Components Analysis

S. Zerbini, F. Raicich, B. Richter, V. Gorini, M. Errico

► **To cite this version:**

S. Zerbini, F. Raicich, B. Richter, V. Gorini, M. Errico. Hydrological Signals in Height and Gravity in Northeastern Italy inferred from Principal Components Analysis. *Journal of Geodynamics*, 2010, 49 (3-4), pp.190. 10.1016/j.jog.2009.11.001 . hal-00615315

**HAL Id: hal-00615315**

**<https://hal.science/hal-00615315v1>**

Submitted on 19 Aug 2011

**HAL** is a multi-disciplinary open access archive for the deposit and dissemination of scientific research documents, whether they are published or not. The documents may come from teaching and research institutions in France or abroad, or from public or private research centers.

L'archive ouverte pluridisciplinaire **HAL**, est destinée au dépôt et à la diffusion de documents scientifiques de niveau recherche, publiés ou non, émanant des établissements d'enseignement et de recherche français ou étrangers, des laboratoires publics ou privés.

## Accepted Manuscript

Title: Hydrological Signals in Height and Gravity in Northeastern Italy inferred from Principal Components Analysis

Authors: S. Zerbini, F. Raicich, B. Richter, V. Gorini, M. Errico



PII: S0264-3707(09)00152-5  
DOI: doi:10.1016/j.jog.2009.11.001  
Reference: GEOD 950

To appear in: *Journal of Geodynamics*

Received date: 23-1-2009  
Revised date: 28-10-2009  
Accepted date: 10-11-2009

Please cite this article as: Zerbini, S., Raicich, F., Richter, B., Gorini, V., Errico, M., Hydrological Signals in Height and Gravity in Northeastern Italy inferred from Principal Components Analysis, *Journal of Geodynamics* (2008), doi:10.1016/j.jog.2009.11.001

This is a PDF file of an unedited manuscript that has been accepted for publication. As a service to our customers we are providing this early version of the manuscript. The manuscript will undergo copyediting, typesetting, and review of the resulting proof before it is published in its final form. Please note that during the production process errors may be discovered which could affect the content, and all legal disclaimers that apply to the journal pertain.



29 contributors to the observed variations. A regional scale signal has been identified in the  
30 GPS station heights; it is characterized by the opposite behavior of the southern and  
31 northern stations in response to the hydrological forcing. At Medicina, in the southern Po  
32 Plain, the EOF analysis has shown a marked common signal between the GPS heights  
33 and the Superconducting Gravimeter (SG) data both over the long and the short period.

34

35 *Keywords:* GPS height; gravity; hydrology; subsidence; Empirical Orthogonal Functions;  
36 Singular Value Decomposition method

37

## 38 **1.0 Introduction**

39

40 The long (multi year) and short (seasonal to a few years) period oscillations  
41 observed in the continuous time series of GPS heights and gravity result from the  
42 superimposition of various phenomena of different physical nature. Among them,  
43 tectonics and the mass transport in the Earth's system which induces deformation of the  
44 Earth's crust in response to variations of the load due to hydrology, air pressure and non-  
45 tidal oceanic effects. Continuous GPS time series exceeding a decade are now available  
46 which can provide reliable information on the long-term height evolution (linear and non-  
47 linear) as well as on the short-period seasonal fluctuations. However, it is complicated to  
48 unravel the contribution of the different components in the observed long-term height  
49 behavior because, at global scale, the Glacial Isostatic Adjustment (GIA) is the only  
50 coherent geological contribution to height variation for which understanding of the  
51 physical process has been achieved. Superconducting gravimeter and/or absolute gravity

52 measurements are not as widely spread as those of GPS, but where both types of  
53 measurements are available, they offer a unique means to detect and understand mass  
54 contributions.

55 It was shown that hydrological mass variations play a major role in the seasonal  
56 height and gravity variability (van Dam et al., 2001; Zerbini et al., 2007). On long-time  
57 scales, climate-related variations of GPS heights and gravity have not yet been clearly  
58 identified mainly because of the limited temporal extent of most of the continuous series  
59 and for the lack of information on the spatial and temporal variability of groundwater  
60 storage.

61 We have studied the variations observed during the last decade in the GPS heights,  
62 gravity and the hydrological time series in northeastern Italy (Fig. 1), as well as their  
63 mutual relationships. The investigated area is affected by both natural and human-  
64 induced subsidence. The Po Plain is a subsiding sedimentary basin encompassed by the  
65 Alps, Apennines and Dinarides Chains. Two structural environments occur within the  
66 basin: the north-verging Apennine fold-and-thrust belt system that is buried under the  
67 Plio-Quaternary cover and a platform gently dipping from the Alps into the basin  
68 (Carminati and Martinelli, 2002). Sedimentation has filled the basin with alternate  
69 stratigraphic sequences of sands, silts and clays variably interbedded and normally  
70 consolidated and containing water in the form of impregnating water and groundwater  
71 (Zerbini et al., 2000; 2002). These conditions are most favorable for the development of  
72 both natural and anthropogenic subsidence. Long-term natural subsidence rates range  
73 between 1-to-2 mm/yr (Pignone et al., 2008), with maximum rates of 2.5 mm/yr  
74 evaluated from the analysis of borehole stratigraphies and from available seismic sections

75 (Carminati et al., 2003) with the largest rates occurring in the southern part of the Po  
76 Plain and in the Po Delta. As discussed by Carminati and Di Donato (1999),  
77 backstripping analysis suggests that tectonics accounts for about 50% of the long-term  
78 natural subsidence, whereas compaction and sediment load account for about 30 and  
79 20%, respectively. However, the present-day geodetic observations show subsidence  
80 rates with peaks up to 40 mm/yr resulting from an anthropogenic component  
81 superimposed to the natural subsidence. The anthropogenic contribution has been  
82 generated by systematic exploitation of groundwater for both industrial and civil use for  
83 about 50 years starting during 1950s. Groundwater control policies have been adopted  
84 since the beginning of the 1980s with the consequent reduction of fluids withdrawal.

85 In our study, we have adopted the Empirical Orthogonal Functions (EOF) and the  
86 Singular Value Decomposition (SVD) analyses. Significant common patterns in the  
87 spatial and temporal variability of GPS heights, gravity and hydrological parameters have  
88 been identified. In particular, hydrology-induced variations are clearly observable starting  
89 in 2002-2003 in the southern part of the Po Plain for the longest GPS time series as well  
90 as for gravity, and from 2005 for the GPS heights over the whole area. Observing and  
91 modeling long- and short-period signals in the height and gravity time series allows to  
92 better understand and quantify subsidence. This knowledge is important because of the  
93 relevant societal impacts of this phenomenon.

94

## 95 **2.0 Data**

96

97 In northeastern Italy, several data sets are available that can be used for a  
98 spatial/temporal analysis of potentially common signals. These are time series of GPS  
99 heights, hydrological information, such as precipitation, simplified hydrological balance  
100 (precipitation minus evapotranspiration) and water table data, and series of absolute  
101 gravity and superconducting gravimeter measurements. Four of the GPS time series are  
102 rather long (about a decade or longer) and continuous.

103

## 104 **2.1 GPS**

105

106 We have used the continuous GPS data of a network located in northeastern Italy  
107 (Fig. 1 and Table 1). The observations were analyzed by means of the Bernese software  
108 package version 5.0 (Dach et al., 2007). The data were processed by using high-accuracy  
109 International GNSS Service (IGS) products including the ionospheric files, the satellite  
110 orbits and the Earth rotation parameters. The ITRF2005 coordinates and velocity field  
111 (Altamimi et al., 2007) were adopted for five IGS stations in Europe (ZIMM, GRAZ,  
112 MEDI, MATE and CAGL) used as fiducial sites in the network adjustment procedure. In  
113 Medicina, there are two GPS receivers, MEDI and MSEL, installed at a distance of about  
114 30 m from each other. Both MEDI and MSEL are EUREF EPN stations. One important  
115 aspect is that the antennas/receivers of the stations, except for MEDI, were never  
116 substituted during the time period of the present analysis. This ensures a desirable  
117 homogeneity of the height series and the absence of jumps due to a change of  
118 instrumentation. The MEDI height time series presented in this paper for comparison  
119 purposes is a EUREF solution kindly provided by K. Szafranek and A. Kenyeres (2009).

120

121 **2.2 Hydrology**

122

123 For all stations, we have estimated a simplified daily hydrological balance. The data  
124 used were the daily precipitation and maximum and minimum air temperature to derive  
125 estimates of the potential evapotranspiration according to the Hargreaves equation  
126 (Hargreaves and Samani, 1982, 1985). In addition, at Medicina, continuous  
127 measurements of the surficial water table are available.

128 In order to compare the hydrological balance data with those of GPS heights and  
129 gravity, we have built hydrological time series in which the n-th element is the time  
130 integral of the daily values from 1 (first epoch) to n. The linear trends have been removed  
131 from these time series in order to highlight the seasonal to interannual variability of the  
132 local hydrology. The residuals turn out to be useful proxies for the surficial water table  
133 fluctuations. Precipitation, treated in the same way as the hydrological balance, also  
134 appears to be a good proxy for the multi-year behavior of the water table. The  
135 identification of reliable proxies is necessary because water table data are not, in general,  
136 readily available. Figure 2 illustrates, as an example for the Medicina station, a  
137 comparison between hydrological balance, precipitation and water table data residuals.  
138 The three series are in good agreement as regards the long-term behavior and the phase of  
139 the seasonal cycle. However, the amplitude of the oscillations of the water table is not  
140 always well represented by the hydrological balance and precipitation.

141

142 **2.3 Gravity**



143

144 Superconducting gravimeter (SG) and absolute gravity (AG) observations are  
145 performed at Medicina, while in Loiano, Bologna, Voltabarozzo, Marghera, Cavallino  
146 and Treviso only AG measurements are carried out (Table 1). The continuous SG  
147 measurements at Medicina start at the beginning of 1998. An instrumental linear drift  
148 ( $18.6 \text{ nms}^{-2}/\text{yr}$ ) was estimated by comparison with a series of AG measurements  
149 performed by means of FG-5 instruments. The gravity data have been analyzed according  
150 to the description given in Zerbini et al. (2007).

151

### 152 **3.0 Methods: EOF and SVD analyses**

153

154 Our objective is twofold: we aim at recognizing both spatial and temporal variability  
155 patterns. We will study the behaviour of individual variables, namely GPS height,  
156 gravity, precipitation, hydrological balance and water table and of variable pairs, for  
157 example, GPS height and precipitation. The analysis is performed using a principal  
158 component approach.

159 In particular, following the terminology proposed by Björnsson and Venegas (1997)  
160 and Venegas (2001), the EOF method is used to analyse individual variables and the  
161 SVD method for variable pairs. It should be mentioned that the terminology is not  
162 univocal in the literature. The EOF and SVD techniques are widely used in geophysics to  
163 analyse temporally and spatially varying fields allowing transforming the data into a  
164 different set with some desirable properties (for more details, see Bretherton et al. (1992),

165 von Storch and Navarra (1999), Björnsson and Venegas (1997), Venegas (2001) and  
166 Hannachi (2004)).

167 The variability of geophysical fields is the result of complex nonlinear interactions  
168 between very many degrees of freedom, and a challenging task is to discriminate between  
169 signal and noise. The definition of signal and noise depends on the specific object of  
170 interest, but, in general, the signal can be a pattern in space and/or time, while the noise,  
171 physical or instrumental, consists of features that are not relevant for the signal.  
172 Normally, the signal has larger temporal and spatial scales and fewer degrees of freedom  
173 than the noise.

174 The EOF analysis provides a compact description of the temporal and spatial  
175 variability of a data set of a single variable in terms of orthogonal components or, also  
176 called, statistical “modes”. Conceptually, the decomposition in EOFs is analogous to,  
177 e.g., those in Fourier periodic functions or Legendre polynomials. The difference is that  
178 the EOF basis functions are not analytic but empirical; the members are not chosen on  
179 analytical considerations, but on maximization of the data projection on them. The first  
180 EOF is selected to be the pattern on which the data project most strongly. In other words,  
181 the leading EOF is the pattern most frequently realized. The second mode is the one most  
182 commonly realized under the constraint of orthogonality to the first one, the third is the  
183 most frequently realized pattern that is orthogonal to both higher modes, and so on.

184 Each EOF is associated to a percentage of the total variance (PVE, percent variance  
185 explained) of the original data set, which accounts for the relative importance of the  
186 corresponding mode of variability. This allows recognizing dominant modes, which are  
187 likely to compose the signal, leaving out the remainder, which is the noise.

188 Let  $f(x,t)$  be the variable of interest, defined at  $n$  locations  $(x_1, \dots, x_n)$  and at  $m$  times  
 189  $(t_1, \dots, t_m)$ . The data are usually arranged in a  $m \times n$  matrix ( $F$ ), where each of the  $n$  columns  
 190 represents the time series for a given location, and each of the  $m$  rows represents the  
 191 spatial distribution at a given time.  $F$  can be written as:

192

193

$$F = U\Gamma V^T$$

194

195  $\Gamma$  is a rectangular ( $m \times n$ ) matrix with positive or zero elements on the diagonal ( $\gamma_k$ ,  
 196  $k=1, \dots, \min(m,n)$ ) and zeroes elsewhere.  $U$  is a ( $m \times m$ ) quadratic matrix, whose  
 197 columns ( $u^k$ ) are orthogonal and represent the EOFs, (or modes or patterns, functions of  
 198 space only).  $V^T$  is a ( $n \times n$ ) quadratic matrix, whose rows ( $v^{Tk}$ ) are also orthogonal and  
 199 represent the principal components (functions of time only).

200 The original field can be reconstructed as a linear combination of all the modes:

201

$$F_m(t) = \sum_k u_m^k a_k(t)$$

202

203 where  $a_k(t) = \gamma_k v^{Tk}(t)$ . Since, in the literature, the nomenclature of the quantities involved  
 204 in the analysis is not univocal, we will call  $u^k$  the “spatial patterns” and  $a_k$  the “time  
 205 components”.

206

207

208

The SVD technique has the same purpose as the EOF, but each component describes  
 a mode of coupled variability of two fields. Similarly to the EOF, each SVD is associated  
 to a percentage of total covariance (SCP, squared covariance percentage).

209

210

The strength of the coupling for each SVD can be quantified by estimating the  
 correlation coefficient between the relevant time components. In order to assess the

211 confidence level of such correlation, we need the number of independent data pairs ( $N_{ind}$ )  
212 involved (i.e. the number of degrees of freedom). In our case, a rigorous estimate is  
213 difficult, therefore we adopt the following definition:  $N_{ind} = N_{tot}T_d / T$ . Here  $N_{tot}$  is the  
214 number of available data pairs,  $T_d$  the “decorrelation time”, namely the first zero of the  
215 time autocovariance function of the involved variables, and  $T$  the length of the time  
216 interval covered by all the data. In the present analysis, the GPS data exhibit quite larger  
217  $T_d$  values (1.2-1.3 years) than the hydrological balance does (about 0.4 years) and  
218 precipitation (about 0.5 years). As a consequence, the number of independent data pairs is  
219 approximately reduced by a factor of 20, when the hydrological balance is involved, or  
220 by a factor of 30, in the case of precipitation.

221 It shall be pointed out that these analyses are purely statistical; therefore the  
222 physical interpretation of the individual components requires specific arguments.

223

#### 224 **4.0 Linear trends: GPS height, gravity and hydrology**

225

226 All stations, except Loiano, which is on the uprising chain of the Apennines, are  
227 located in the Po Plain and northeastern Adriatic; this area is characterized by relevant  
228 natural subsidence. The largest rates are mainly of anthropogenic nature (Zerbini et al.,  
229 2007). Figure 3 presents the time series of the GPS heights in the ITRF2005 and the AG  
230 and SG gravity series of the stations in the network. Gravity has been multiplied by a  
231 factor (-1) in order to facilitate the visual comparison with the height data. The height  
232 time series show a decrease in the subsidence rates starting around 2004-2005; an  
233 exception is San Felice which, instead, exhibits an increase in subsidence. Table 1 lists,

234 both for GPS and gravity, the linear trends computed over the entire time span. The  
235 formal errors associated to the linear trend estimates both of GPS height and gravity have  
236 been multiplied by an arbitrary factor of 5 in order to provide a conservative estimate of  
237 the errors. Figure 3d concerns the Medicina station. It presents the MEDI and MSEL GPS  
238 height series as well as the SG and AG gravity observations multiplied by (-1). The two  
239 GPS series and those of gravity are comparable. They all show from about 2005 a  
240 different long-term behavior, a reduction of subsidence, with even a tendency to uplift  
241 during the last two years 2006-2007.

242 In Bologna (EUREF EPN station BOLG, Figure 3c), the linear trend turns out to be  
243  $-10.57 \pm 0.25$  mm/yr for the period 1999-2008 and  $-8.31 \pm 0.40$  mm/yr in the time frame  
244 2002-2008 corresponding to the period for which absolute gravity measurements are also  
245 available. The trend estimated from the gravity data is  $+4.17 \pm 1.75$   $\mu$ Gal/yr, consistent  
246 with the GPS results, within the statistical error, if using the free-air conversion factor  
247 (Vaníček and Krakiwski, 1986). The free-air relation mostly occurs locally (Torge,  
248 1989).

249 In the Bologna area, data acquired with the Interferometric Synthetic Aperture Radar  
250 (InSAR) technique are available. In a previous work (Zerbini et al., 2007), a first  
251 comparison was made between the GPS and InSAR subsidence rates which showed the  
252 consistency of the two estimates. A recent analysis of InSAR observations (Ferretti,  
253 T.R.E., 2009), allows a further comparison supporting the reduction in the subsidence  
254 rate observed by GPS at the BOLG station. T.R.E. kindly provided us with the results of  
255 their Permanent Scatterers (Ferretti et al., 2001) analysis for two different periods and  
256 satellites images. Figure 4 (a) shows the InSAR results obtained using the ERS satellite

257 images for the period 1992-2000 and (b) the RADARSAT passes in the time frame 2003-  
258 2007. The comparison between the two images indicates a major reduction in the  
259 subsidence rate over the Bologna area in the latter period.

260 The stations around the Venice area (Fig. 3 f, g, h, i and j) show reasonable agreement  
261 between the GPS and AG linear trends. However, it should be pointed out that the AG  
262 series are still limited in time and the associated errors, in particular for Marghera and  
263 Cavallino, located a few hundred meters from the sea shore, are rather large.

264 The main hydrological parameters used in this work are the integrated simplified  
265 hydrological balances and the precipitation series as described in section 2.2. In order to  
266 achieve an understanding of the long-period behavior of the regional hydrology, we  
267 estimated the linear trend of the hydrological balance for all stations over the period  
268 1998-2007. It was found that, over this decade, only the northern stations at Treviso  
269 ( $+362\pm 4$  mm/yr), Voltabarozzo ( $+35\pm 3$  mm/yr) and Cavallino ( $+38\pm 3$  mm/yr) gain water,  
270 while in all other sites, the amount of water is decreasing. In particular, the stations  
271 located in the Plain, south of the Po River (Medicina, Marina di Ravenna, Bologna and  
272 Boretto), are characterized by large negative trends up to  $-500$  mm/yr. The analysis of the  
273 precipitation series shows similar results.

274

## 275 **5.0 Long-period oscillations**

276

277 Many authors have shown that short-period (seasonal) height and gravity oscillations  
278 are related to seasonal mass variations (see, for example, Blewitt et al., 2001; van Dam et

279 al., 2001; Zerbini et al., 2007). On the other hand, long-period (multi year) variations are  
280 not as yet well understood because of the limited length of most of the time series.

281 In order to identify long-period oscillations, both the GPS heights and the  
282 hydrological series were detrended to derive the residuals (Fig. 5). Possible correlations  
283 between these residuals were investigated. For the sake of clarity, we point out that we  
284 identify as hydrological balance and precipitation residuals the detrended series of the  
285 time integral values of the observed hydrological balance and precipitation respectively.  
286 Linear regressions were calculated between the height and the corresponding  
287 hydrological balance and precipitation residual values.

288 By considering the Marina di Ravenna and Medicina residuals (Fig. 5b and d), over  
289 the long period (multiyear), we observe anticorrelation between the height and each of  
290 the two hydrological parameters. Anticorrelation can be interpreted as the loading effect  
291 on the Earth's crust caused by the hydrology. In particular, for the MSEL station, a  
292 regression between the hydrological balance and the height residuals over the period  
293 1996-2008 provides a ratio of  $-24.7 \pm 0.7$  (significant at 99% confidence level), which  
294 implies that for an increase of 24.7 mm of hydrological balance there is 1 mm decrease in  
295 height (loading effect). A similar result is obtained by using the precipitation data  
296 ( $-18.6 \pm 0.4$ , 99% confidence level). At Marina di Ravenna, on the Adriatic coast, the  
297 ratios turn out to be  $-7.9 \pm 0.4$  and  $-8.1 \pm 0.2$  for the hydrological balance and the  
298 precipitation residuals respectively. Since this site is on the coast, the magnitude of the  
299 loading effect turns out to be smaller than that of the inland site (van Dam et al., 1994), in  
300 this case about a factor of 2-to-3 of that observed inland at Medicina. The BOLG station  
301 height residuals are characterized by a positive although weak correlation,  $+3.3 \pm 0.4$  and

302 +4.1±0.2, with the hydrological balance and precipitation residuals respectively. All the  
303 northern stations exhibit positive correlation. Since correlation is not explained by  
304 loading, different physical mechanisms shall be invoked. A possible explanation could be  
305 provided by the buoyancy effect according to which an increase/decrease of the  
306 groundwater amount in the soil would produce an increase/decrease of height. Also clay  
307 swelling/shrinking on water uptake/loss may occur. The different observed behaviors can  
308 be related to the different geological settings and to the environmental conditions.

309

## 310 **6.0 Regional analysis**

311

312 The residual series of the GPS heights and gravity were analyzed both individually  
313 and in conjunction with hydrological parameters by means of the EOF and SVD  
314 approaches. We performed an EOF analysis on the individual variables, namely GPS  
315 height, precipitation and hydrological balance, in order to identify spatial and temporal  
316 variability features at local and regional scales. Additionally, at Medicina, the EOF  
317 analysis has been carried out between pairs of variables: GPS height and water table,  
318 gravity and hydrology, GPS height and gravity. The SVD analysis has been applied to  
319 detect common signals between GPS heights and precipitation as well as between GPS  
320 heights and hydrological balance. The length of the time series is an important factor  
321 because only three GPS stations are present for a decade or longer, while all the stations  
322 are simultaneously available only from 2004.

323 In order to reduce the high-frequency variability, the analysis is performed on weekly  
324 time series. The weekly values were obtained by averaging the original daily data. A



325 weekly mean was computed when at least four daily values were available. Gaps shorter  
326 than three days were preliminarily interpolated using the Objective Analysis technique  
327 (Gandin, 1965; Bretherton et al., 1976).

328 The EOF and SVD analyses require that all series be defined at the same epochs; the  
329 time series were detrended over the common period. Since variables measured in  
330 different units may be involved, all the residual time series were standardized to zero  
331 mean and unit standard deviation.

332 In the following, several cases were considered. Since we are interested in  
333 understanding the long-period variability observed both in the height and gravity data,  
334 only the stations with observation periods longer than six years were analyzed. We point  
335 out that the gaps in the EOFs series are mostly due to missing GPS data at the Boretto  
336 station. We will discuss spatial patterns, i.e. the coefficients shown in Tables 2 through 5  
337 for the EOF analysis and Tables 6 and 7 for the SVD method, and time components, i.e.  
338 the curves shown in Figures 6 and 7 for the EOF and Figure 8 for the SVD. For each  
339 case, we will comment only the two largest EOFs (EOF1 and EOF2) and SVDs (SVD1  
340 and SVD2) because, in general, they explain most of the observed variance. However,  
341 Tables 2 to 7 list the whole set of EOF and SVD spatial patterns.

342

### 343 **6.1 GPS height series**

344

345 *Case A - Five GPS stations (1999-2007)*

346

347 In this case, identified as case A, we analyse the GPS height time series of five  
348 stations: MSEL, MEDI, Marina di Ravenna, BOLG and Boretto. These sites are located  
349 in the southern part of the region and are characterized by the longest data records,  
350 spanning about eight years, from 1999 to the end of 2007. Concerning EOF1, the spatial  
351 pattern shows that all stations behave coherently (Table 2). A height increase is observed  
352 starting 2004-2005. A clear seasonality is superimposed with summer maxima and winter  
353 minima (Fig. 6a). The spatial pattern of EOF2 is characterized by opposite behaviours of  
354 Medicina (both MSEL and MEDI) and Boretto on one side, and Marina di Ravenna and  
355 BOLG on the other. The EOF2 time component also shows a long-term signal, the slope  
356 inversion starting around 2004.

357

358 *Case B - Eight GPS stations (2001-2007)*

359

360 Here we consider the stations of the previous case plus Cavallino, San Felice and  
361 Voltabarozzo. In this case, called case B, eight stations are simultaneously available for a  
362 period of about six years, from 2001 through the end of 2007, thus allowing us to extend  
363 the analysis to the northern part of the region. Both EOF1 and EOF2 time components  
364 show a long-term change starting around 2004-2005 (Fig. 6b). However, the EOF1  
365 spatial pattern exhibits a different behaviour if we compare the northern and southern  
366 stations (Table 3): while the northern sites have winter height maxima, the southern ones,  
367 except BOLG, exhibit minima. Instead, the EOF2 spatial pattern is coherent across the  
368 whole region.

369

370 **6.2 Precipitation time series**

371

372 The two cases described previously for the GPS heights are now considered for the  
373 precipitation time series. It shall be pointed out that, for the Medicina site, we deal with a  
374 unique precipitation series since the two GPS receivers (MEDI and MSEL) are separated  
375 by 30 m only. Moreover, for Marghera, the precipitation data are not available.  
376 Therefore, we will analyze two cases with four and seven stations respectively. Both  
377 analyses show that EOF1 explains at least 75% of variance.

378

379 *Four precipitation stations (1999-2007)*

380

381 The Medicina, Marina di Ravenna, Bologna and Boretto precipitation series are  
382 analyzed during the period 1999-2007. These precipitation stations are identified in the  
383 relevant Tables with the abbreviations ME, RA, BO and BR respectively. EOF1 is  
384 characterized by a coherent spatial pattern and by significant interannual fluctuations  
385 (Table 4 and Fig. 7a). Considerable precipitation minima are found in 1999, 2002, 2003  
386 and 2007 and maxima during the winters 1999-2000, 2002-2003 and during most of  
387 2006. In Medicina and Bologna, EOF2 exhibits a decrease until 2003-2004, followed by  
388 an increase; the opposite is found in Marina di Ravenna and Boretto.

389

390 *Seven precipitation stations (2001-2007)*

391

392 Cavallino, San Felice and Voltabarozzo precipitation time series are considered in  
393 addition to the four stations mentioned above; in the Tables they are identified by means  
394 of the following abbreviations: CA, SF and VO respectively. The results are quite similar  
395 to those of the previous case (Table 5 and Fig. 7b).

396

### 397 **6.3 Hydrological Balance time series**

398

399 We analyzed also the hydrological balance time series by following the same scheme  
400 used for the precipitation data described above. EOF1s, explaining about 90% variance,  
401 are characterized by spatial coherence over the entire region. The related time  
402 components exhibit a clear seasonality. The EOF2s are comparatively much smaller than  
403 those in the case of precipitation.

404

### 405 **6.4 GPS height and precipitation**

406

407 The coupled variability of GPS height and hydrological variables (precipitation and  
408 hydrological balance) is studied by using the SVD approach. Within the SVD analysis we  
409 also distinguish two cases.

410

411 *Five GPS and four precipitation stations (1999-2007)*

412

413 We analyze the GPS heights of case A together with the Medicina, Marina di  
414 Ravenna, Bologna and Boretto precipitation series for the period 1999-2007. SVD1

415 explains 81% covariance; the precipitation spatial pattern is characterized by coherence  
416 (Table 6b). The GPS height spatial pattern is anticorrelated with precipitation at Medicina  
417 (both MSEL and MEDI) and Boretto, while RA and BOLG do not show significant  
418 correlation (Table 6a). Both time components exhibit a long-period fluctuation, with a  
419 minimum around 2003-2004 (Fig. 8a), superimposed to which are seasonal oscillations.  
420 The anticorrelation can be interpreted as a loading/unloading effect on the Earth's crust  
421 caused by variations in the precipitation regime. The SVD2 spatial pattern of the GPS  
422 height mostly exhibits regional coherence. Both time components show a long-term  
423 fluctuation with a seasonal signal superimposed. GPS is characterized by decreasing  
424 heights until beginning of 2004 and by an increase afterwards.

425 The correlation coefficients between the relevant SVD time components turn out to  
426 be 0.45 for SVD1 and 0.65 for SVD2, SVD1 significant at 93% confidence level while  
427 SVD2 significance is greater than 99%.

428

429 *Eight GPS and seven precipitation stations (2001-2007)*

430

431 Here we analyze the GPS heights of case B together with the seven precipitation  
432 series mentioned above. The time span thus reduces to 2001-2007. The covariance  
433 explained by SVD1 amounts to about 92%. The precipitation spatial pattern is coherent  
434 (Table 7b), while the GPS height pattern is characterized by a dipole (Table 7a). As  
435 regards the northern stations, GPS heights are correlated with precipitation, while the  
436 southern ones are anti-correlated. SVD2 shows a low percentage of covariance (6%). A  
437 long-term fluctuation is clearly recognizable in both SVDs with characteristics similar to

438 those of the previous case (Fig. 8b). Here, the correlation coefficients are 0.45 for SVD1  
439 and 0.64 for SVD2, the first is significant at 90% confidence level while the significance  
440 of the second is 98%.

441 Since SVD1 explains more than 90% of the signal and the GPS height pattern  
442 exhibits a well-defined south-north asymmetry, we further investigated the relationship  
443 between the GPS height and precipitation. After estimating the average standard  
444 deviations of the two parameters for the southern and northern parts of the region  
445 respectively, we have computed the relevant ratios indicative of the height response to  
446 precipitation variations. In the south, the ratio turns out to be 1 mm of height for 20 mm  
447 of precipitation. In the north the ratio is instead 1/35. Because, by definition, the standard  
448 deviation is a positive quantity, the signs are deduced from those of the relevant SVD1  
449 spatial patterns (Table 7); therefore in the south the sign of the ratio is negative whereas  
450 in the north it is positive. These values are in agreement with those derived by means of  
451 linear regressions between height and precipitations residuals (see section 5.0). If we  
452 assume a 1 mm homogeneous increase of precipitation over the entire area, there would  
453 be about 0.05 mm height decrease in the southern part while a height increase of about  
454 0.03 mm would occur in the north.

455

## 456 **6.5 GPS height and hydrological balance**

457

458 The coupled variance between GPS height and hydrological balance exhibits results  
459 quite similar to those obtained by using precipitation. In all these analyses, the SVD1s  
460 explain a slightly larger covariance compared to the same cases involving precipitation.

461 The spatial patterns of the hydrological balance are always regionally coherent; however,  
462 as in section 6.4, the GPS heights of the northern stations are correlated with the  
463 hydrological balance, while the southern ones are anti-correlated except for BOLG.

464

## 465 **7.0 Local scale analysis - Medicina**

466

467 At Medicina, time series of various parameters are acquired continuously for more  
468 than a decade now, GPS height (MSEL and MEDI stations), SG gravity, water table data  
469 and other environmental information. This makes it possible to compare locally the  
470 different series. A few examples are provided, namely we correlate, by means of the EOF  
471 analysis, GPS height (both MEDI and MSEL) with water table, SG gravity with  
472 precipitation and water table respectively and GPS height and SG gravity. Tables 8  
473 through 10 present the pattern coefficients while the time components are presented in  
474 Figures 9, 10 and 11.

475

### 476 **7.1 GPS height and water table**

477

478 The two GPS height data sets, MSEL and MEDI, exhibit the same response to the  
479 water table variations (Fig. 9a and b, Table 8a and b). Both EOF1s are clearly  
480 representative of the loading/unloading effect caused by the seasonal water table  
481 variations. We observe maxima in the summer when the water table decreases and  
482 minima in the winter when the water table rises close to the topographic surface. This  
483 comparison also allows identifying a height decrease starting in 2002-2003 followed by a

484 height increase starting at the end of 2005. These long-period height variations are  
485 correlated with increase/decrease in the water table level as a consequence of changes in  
486 the precipitation regime.

487

## 488 **7.2 SG gravity and hydrology**

489

490 We have compared the SG data series with those of precipitation and water table. The  
491 results provided by the two cases are similar (Fig. 10a and b; Table 9a and b), although  
492 the SG data are slightly more correlated with the water table variations (63.6% PVE) than  
493 to those of precipitation (52.7% PVE). Both EOF1s show a clear seasonal signal with  
494 summer minima and winter maxima likely resulting from the combination of two effects:  
495 the variations in gravity due to the Newtonian mass attraction and to height fluctuations.  
496 In fact, the EOF1s pattern coefficients have the same sign indicating on the one hand that  
497 to an increase/decrease of water mass corresponds an increase/decrease of gravity; on the  
498 other hand an increase of water/precipitation will load the crust inducing a height  
499 decrease, which turns into a gravity increase. In the case of the EOF2s, we can notice a  
500 long-period signal starting at the beginning of 2002-2003. The pattern coefficients of  
501 EOF2s have opposite sign; this mode could be explained by invoking a variation in  
502 gravity due to a height change resulting from a buoyancy effect and/or a soil  
503 consolidation process. In this latter case, a decrease of the water content in the soil will  
504 cause a height decrease which, in turn, will result into a gravity increase. The soil  
505 consolidation phenomenon is known to occur particularly in clayey soils such as that  
506 present at Medicina (Romagnoli et al., 2003).



507

### 508 **7.3 GPS height and SG gravity**

509

510 The EOF1s time components for MEDI and MSEL show a clear seasonal signal both  
511 in GPS heights and SG time series (Fig. 11a and b) as well as a long-period feature  
512 starting at the beginning of 2005. The pattern coefficients are of opposite sign (Table 10a  
513 and b), thus indicating anticorrelation between the two variables for the EOF1s. This  
514 means that the seasonal maxima and minima of GPS heights and SG gravity are opposite  
515 in phase as expected, and that, on a longer period of time, to the height increase starting  
516 in 2005 corresponds a gravity decrease. The EOF2s indicate the presence of a long-period  
517 oscillation with a minimum around 2002-2003. The pattern coefficients have the same  
518 sign (Table 10a and b) suggesting that this mode could result from buoyancy and/or soil  
519 consolidation effects.

520

### 521 **8.0 Comparisons**

522

523 We compared, as an example, the original detrended GPS height series and the  
524 reconstructed signals by means of the main EOFs components for the two cases A and B  
525 (see section 6.1). According to our arbitrary choice, the reconstructed signals must  
526 explain at least 70% of the observed variance. Therefore, three EOFs were used in case  
527 A, thus accounting for 70.2% of the variance (Table 2 and Fig. 12). In case B, five EOFs  
528 were selected which represent 78.9% of the variance (Table 3 and Fig. 13). For the  
529 stations which are common to cases A and B, there are no major differences between the

530 two EOF reconstructions. However, it shall be noticed that in case A (Fig. 12) Marina di  
531 Ravenna shows, in the period 2004-2006 a minor discrepancy between the observed  
532 height residuals and the reconstructed signal, which does not appear in case B (Fig. 13).  
533 This difference might be due to the fact that the reconstruction of the signal in case B is  
534 accomplished through a slightly larger variance (78.9%) with respect to A (70.2 %). In  
535 case B, the analysis is also covering a larger area with respect to A; this might imply the  
536 presence of an additional regional component.

537

## 538 **9.0 Conclusions**

539

540 Over northeastern Italy, starting around 2004-2005, a reduction of the subsidence  
541 rates has been observed in conjunction with a decrease of the hydrological load on the  
542 Earth's crust mostly due to a decrease in the amount of precipitation.

543 The EOF and SVD analyses of the residuals of the GPS heights, hydrological  
544 parameters and gravity made it possible to identify long and short period oscillations and  
545 also to recognize common features in different pairs of variables. These findings,  
546 obtained by means of purely mathematical approaches, are supported by sound physical  
547 interpretation that allows to point at the local/regional hydrology as one of the main  
548 contributors to the observed height oscillations. Since a percentage of variance or  
549 covariance is associated to each EOF or SVD component respectively, the mathematical  
550 decomposition of the time series, together with the physical interpretation, provides a  
551 means to attribute a relative weight to the different phenomena involved.

552 In both the analyzed A and B cases (section 6.1), the time components of the main  
553 EOFs show a slope inversion starting around 2004-2005. In particular, a coherent height  
554 increase is found by EOF1 in case A (Fig. 6a, Table 2) and by EOF2 in case B (Fig. 6b,  
555 Table 3). Also the EOF1 spatial pattern in case B clearly indicates an opposite north-  
556 south behavior of the station heights on the short as well as on the multi-year period  
557 (Table 3). For example, at seasonal scale, this means that summer height maxima of the  
558 stations in the southern Po Plain are mirrored by height minima in the northern part of the  
559 region. Case B, which involves a larger spatial domain with respect to case A, has made  
560 it possible to recognize a regional signal.

561 As regards precipitation, the EOF1s of both the four and seven station cases  
562 (section 6.2) show a marked decrease in the precipitation residuals starting at the end of  
563 2005 (Fig. 7a and b and Tables 4 and 5).

564 The SVD analysis of the GPS heights and precipitation series has demonstrated  
565 the high spatial covariance and the high time correlation between these two parameters.  
566 The SVD1 in both analyses indicates that the GPS heights of the sites in the southern Po  
567 Plain are anticorrelated with precipitation, while the northern sites are positively  
568 correlated. We have interpreted anticorrelation as the loading/unloading effect on the  
569 Earth's crust exerted by the increase/decrease in precipitation, which occurs in the period  
570 2002-2005 and 2006-2008 respectively (Fig. 8). The reduction in the precipitation regime  
571 observed, for example, from the end of 2005, unloads the crust and it turns into a height  
572 increase particularly at the stations located in the southern Po Plain which are  
573 characterized mostly by clayey soils.

574 The opposite response to hydrological loading of the southern and northern parts  
575 of the region under investigation (see 6.1, case B and 6.4 “eight GPS and seven  
576 precipitation stations”) results in a south-north height gradient, which turns out to be in  
577 the order of 0.1 mm over a distance of about 100 km, by assuming a 1 mm homogeneous  
578 increase of precipitation over the entire area. When observing and studying crustal  
579 deformation of a region, it is important to identify how the height of the stations changes  
580 in response to the hydrological load, in particular when weak tectonic signals are being  
581 sought.

582 At Medicina, a few comparisons were made, namely between GPS heights and  
583 water table, SG gravity data and hydrology and between GPS heights and SG gravity  
584 (Fig. 10). In all three cases, the EOF1s time components are characterized by a clear  
585 seasonal signal. This is due to loading/unloading of the crust in the case of the GPS  
586 height variations and to variations of Newtonian mass attraction and height in the case of  
587 gravity. GPS height and SG gravity show a marked common seasonal signal as well as a  
588 long-term fluctuation (Fig. 11) pointing to a height increase which is quite evident  
589 starting from the end of 2005.

590

## 591 **References**

592

593 Altamimi, Z., X. Collilieux, J. Legrand, B. Garayt and C. Boucher (2007), ITRF2005: A  
594 new release of the International Terrestrial Reference Frame based on time series of  
595 station positions and Earth Orientation Parameters, *J. Geophys. Res.*, 112, B09401,  
596 doi:10.1029/2007JB004949.

597

598 Björnsson, H. and S. Venegas (1997), A Manual for EOF and SVD Analyses of Climate  
599 Data. CCGCR Report No. 97-1, Montréal, 52 pp (available from [www.awi.de](http://www.awi.de)).

600

601 Blewitt, G., D. Lavallée, P. Clarke and K. Nurutdinov (2001), A new global mode of  
602 Earth deformation: Seasonal cycle detected, *Science*, 294, 2342– 2345.

603

604 Bretherton, F. P., R. E. Davis, and C. B. Fandry (1976), A technique for objective  
605 analysis and design of oceanographic experiments applied to MODE-73, *Deep-Sea Res.*,  
606 23, 559–582.

607

608 Bretherton, C.S., C. Smith, and J.M. Wallace (1992), An intercomparison of methods for  
609 finding coupled patterns in climate data. *J. Climate*, 5, 541–560.

610

611 Carminati, E. and G. Di Donato, (1999), Separating natural and anthropogenic vertical  
612 movements in fast subsiding areas: the Po Plain (N. Italy) case. *Geophys. Res. Lett.* 26,  
613 2291–2294.

614

615 Carminati, E. and G. Martinelli (2002), Subsidence rates in the Po Plain, northern Italy:  
616 the relative impact of natural and anthropogenic causation. *Engineering Geology*, 66, 241–  
617 255.

618

- 619 Carminati, E., C. Doglioni, and D. Scrocca (2003), Apennines subduction related  
620 subsidence of Venice (Italy), *Geophys. Res. Lett.*, 30(13), 1717,  
621 doi:10.1029/2003GL017001.
- 622
- 623 Dach, R., U. Hugentobler, P. Fridez and M. Meindl (2007), Bernese GPS Software  
624 version 5.0, Stämpfli Publications AG Bern, 612 pp.
- 625
- 626 Ferretti, A., C. Prati and F. Rocca (2001), Permanent Scatterers in SAR interferometry,  
627 *IEEE Trans Geosci. Remote Sens.*, 39, 8-20.
- 628
- 629 Ferretti, A., T.R.E. (Tele-Rilevamento Europa T.R.E. srl) (2009), Private communication.
- 630
- 631 Gandin, L. S. (1965), Objective Analysis of Meteorological Fields, Israel Program for  
632 Scientific Translations, 242 pp.
- 633
- 634 Hannachi, A. (2004), A Primer for the EOF Analysis of Climate Data, Department of  
635 Meteorology, University of Reading, UK, 33pp (Available from: [ncas-cms.nerc.ac.uk](http://ncas-cms.nerc.ac.uk))
- 636
- 637 Hargreaves, G.H. and Z.A. Samani (1982), Estimating potential evapo-transpiration. *J.*  
638 *Irrig and Drain Engr.*, ASCE, 108 (IR3), 223-230.
- 639
- 640 Hargreaves, G.H. and Z.A. Samani (1985), Reference crop evapo-transpiration from  
641 temperature. *Transactions of ASAE*, 1 (2), 96-99.

642

643 Pignone, R., U. Cibin, P. Severi (2008), Pianura bolognese e costa le aree più critiche,  
644 Supplemento al N. 1, anno XI, ARPA Rivista, gennaio-febbraio 2008, Il monitoraggio  
645 della subsidenza - Esperienze a confronto, 8-9.

646

647 Romagnoli, C., S. Zerbini, L. Lago, B. Richter, D. Simon, F. Domenichini, C. Elmi, M.  
648 Ghirotti (2003), Influence of soil consolidation and thermal expansion effects on height  
649 and gravity variations, *Journ. of Geodynamics*, 35, N. 4-5, 521-539.

650

651 Szafranek, K. and A. Kenyeres (2009), Private communication.

652

653 Torge, W., (1989), *Gravimetry*, W. De Gruyter, 465 pp.

654

655 Van Dam, T.M., G. Blewitt, M.B. Heflin (1994), Atmospheric pressure loading effects on  
656 Global Positioning System coordinate determinations, *J. Geophys. Res.*, 99(B12), 23.939-  
657 23.950.

658

659 van Dam, T. M., J. Wahr, P.C.D. Milly, A. B., Shmakin, G. Blewitt, D. Lavallée and K.  
660 M. Larson (2001), Crustal displacements due to continental water loading, *Geophys. Res.*  
661 *Lett.*, 28, 4, 651-654, doi: 10.1029/2000GL012120.

662

663 Vaníček, P. and E.J. Krakiwski (1986), *Geodesy: the concepts*, North-Holland,  
664 Amsterdam, 697 pp.

665

666 Venegas, S.A. (2001) Statistical Methods for Signal Detection in Climate. DCESS Report  
667 No. 2, Niels Bohr Institute for Astronomy, Physics and Geophysics, University of  
668 Copenhagen, 96 pp.

669

670 von Storch, H., and A. Navarra (Eds.) (1999), Analysis of Climate Variability:  
671 Applications of Statistical Techniques, Springer Verlag, Berlin, 342 pp.

672

673 Zerbini, S., B. Richter, M. Negusini, D. Simon, C. Romagnoli and F. Domenichini  
674 (2000), Vertical crustal motions and mean sea level: an experiment in the Eastern Po  
675 Plain, in Land Subsidence, Proceedings of the Sixth International Symposium on Land  
676 Subsidence, 24-29 September 2000, Ravenna, Italy, L. Carbognin, G. Gambolati A.I.  
677 Johnson eds., ISBN 88-87222-06-1, vol. II, 151-163.

678

679 Zerbini S., M. Negusini, C. Romagnoli, F. Domenichini, B. Richter, D. Simon (2002),  
680 Multi-parameter continuous observations to detect ground deformation and to study  
681 environmental variability impacts, Global and Planetary Change 34, 37–58.

682

683 Zerbini S., B. Richter, F. Rocca, T. van Dam, F. Matonti, (2007), Combination of space  
684 and terrestrial geodetic techniques to monitor land subsidence: Case study, the  
685 southeastern Po Plain, Italy, Journ. Geophys. Res. Solid Earth, 112, B05401,  
686 doi:10.1029/2006JB004338.

687

688 **Acknowledgments**



689

690 This work has been developed in the frame of the IGCP 565 project “Developing the  
691 Global Geodetic Observing System into a Monitoring System for the Global Water  
692 Cycle”. The authors are grateful to Dr. Erika De Simone for having contributed to the  
693 analysis of the GPS data and to Dr. Hartmut Wziontek and Eng. Peter Wolf for the  
694 analysis of the SG gravity data. We would like to thank Prof. A. Ferretti and T.R.E. for  
695 having provided the InSAR results. We also would like to thank Drs. K. Szafranek. and  
696 A. Kenyeres for having provided the weekly EUREF GPS height solutions of the MEDI  
697 station. The authors are also grateful to two unknown reviewers the comments and  
698 suggestions of which helped us to improve the manuscript.

699

700 Figure Captions

701

702 Figure 1. Map of station locations in northeastern Italy. Bologna, Loiano, Marina di  
703 Ravenna, Medicina (MSEL) are stations of the GPS network run by the University of  
704 Bologna; Boretto belongs to Telespazio; Cavallino, Marghera, San Felice, Treviso and  
705 Voltabarozzo are stations of the GPS network run by Consorzio Venezia Nuova for the  
706 Magistrato alle Acque of Venice; the MEDI station belongs to the Italian Space Agency.

707

708 Figure 2. Medicina: daily water table (cyan line), hydrological balance (red line) and  
709 precipitation (black line) data.

710

711 Figure 3. Time series of GPS heights and gravity; they are ordered from south to north.  
712 Panel a) Loiano (LOIA) daily GPS height (purple line); b) Marina di Ravenna (RA)  
713 daily GPS height (red line); c) Bologna (BOLG) daily GPS height (blue line) and a series  
714 of AG measurements (red dots); d) Medicina GPS heights: MEDI (magenta line, EUREF  
715 weekly solution) and MSEL (olive line, daily solution); daily SG time series (blue line)  
716 and AG measurements (red dots); e) Boretto (BR) daily GPS height (dark yellow line); f)  
717 San Felice (SF) daily GPS height (wine line); g) Voltabarozzo (VO) daily GPS height  
718 (dark green line) and AG measurements (red dots); h) Marghera (MA) daily GPS height  
719 (dark blue line) and AG measurements (red dots); i) Cavallino (CA) daily GPS height  
720 (orange line) and AG measurements (red dots); j) Treviso (TV) daily GPS height (violet  
721 line) and AG measurements (red dots). In all panels, gravity is multiplied by (-1).

722

723 Figure 4. InSAR maps of the terrain deformation in the Bologna area; (a) ERS  
724 descending passes in the period 1992-2000 and (b) Radarsat descending passes during  
725 2003-2007.

726

727 Figure 5. GPS height, precipitation (black line) and hydrological balance (cyan line)  
728 residuals. GPS: Panel a): LOIA (purple line); b) RA (red line); c) BOLG (blue line); d)  
729 MSEL (olive line) and MEDI (magenta line); e) BR (dark yellow line); f) SF (wine line);  
730 g) VO (dark green line); h) MA (dark blue line); i) CA (orange line); j) TV (violet line).

731

732 Figure 6. EOF1 and EOF2 time components of GPS height residuals. Panel a) Five GPS  
733 stations: MSEL, MEDI, RA, BOLG and BR; b) Eight GPS stations: MSEL, MEDI, RA,  
734 BOLG, BR, CA, SF and VO.

735

736 Figure 7. EOF1 and EOF2 time components of precipitation residuals. Panel a) Four  
737 precipitation stations: Medicina (ME), Marina di Ravenna (RA), Bologna (BO) and  
738 Boretto (BR); b) Seven precipitation stations: ME, RA, BO, BR, Cavallino (CA), San  
739 Felice (SF) and Voltabarozzo (VO).

740

741 Figure 8. SVD1 and SVD2 time components of the variable pair GPS height (blue dots)  
742 and precipitation residuals (red dots). Panel a) Five GPS stations (MSEL, MEDI, RA,  
743 BOLG and BR) and four precipitation stations (ME, RA, BO and BR); b) Eight GPS  
744 stations (MSEL, MEDI, RA, BOLG, BR, CA, SF and VO) and seven precipitation  
745 stations (ME, RA, BO, BR, CA, SF and VO).

746

747 Figure 9. EOF1 and EOF2 time components of the Medicina GPS height and water table  
748 residuals. Panel a) MEDI and water table; b) MSEL and water table.

749

750 Figure 10. EOF1 and EOF2 time components of the Medicina superconducting  
751 gravimeter (SG) and local hydrology residuals: Panel a) SG and precipitation; b) SG and  
752 water table.

753

754 Figure 11. EOF1 and EOF2 time components of the Medicina GPS height and  
755 superconducting gravimeter (SG) residuals. Panel a) MEDI and SG; b) MSEL and SG.

756

757 Figure 12. EOF reconstruction and observed height residuals. Five GPS stations: Panel a)  
758 RA, observed height residuals (red line) and EOF reconstruction (green line); b) BOLG  
759 (blue and purple); c) MSEL (olive and orange); d) MEDI (magenta and navy) and e) BR  
760 (dark yellow and cyan). The reconstruction is based on the first three EOFs and explains  
761 70.2% of the total variance.

762

763 Figure 13. EOF reconstruction and observed height residuals. Eight GPS stations: Panel  
764 a) RA, observed height residuals (red line) and EOF reconstruction (green line); b)  
765 BOLG (blue and purple); c) MSEL (olive and orange); d) MEDI (magenta and navy); e)  
766 BR (dark yellow and cyan); f) SF (grey and pink); g) VO (wine and yellow) and h) CA  
767 (dark cyan and black). The reconstruction is based on the first five EOFs and explains  
768 78.9% of the total variance.

769

770

### Table Captions

771

772 Table 1.

773 List of stations, North/South regional identifier, techniques available and linear trends of

774 the GPS height, Superconducting Gravimeter (SG) and Absolute Gravity (AG) series.

775 The formal error associated to the estimated trends, both for GPS heights and gravity,

776 have been multiplied by an arbitrary factor of 5 to provide conservative estimates of the

777 errors. The superscript (a) indicates that only one AG measurement is available at LOIA.

778 The superscript (b) indicates that the MEDI data are EUREF weekly solutions.

779

780 Table 2. EOF analysis of five GPS height residuals series (MSEL, MEDI, RA, BOLG

781 and BR). The second column lists the percentage of variance explained (PVE) by each

782 EOF, the following columns describe the spatial patterns.

783

784 Table 3. EOF analysis of eight GPS height residuals series (MSEL, MEDI, RA, BOLG,

785 BR, CA, SF and VO). The second column lists the percentage of variance explained

786 (PVE) by each EOF, the following columns describe the spatial patterns.

787

788 Table 4. EOF analysis of four precipitation residuals series (ME, RA, BO and BR). The

789 second column lists the percentage of variance explained (PVE) by each EOF, the

790 following columns describe the spatial patterns.

791

792 Table 5. EOF analysis of seven precipitation residuals series (ME, RA, BO, BR, CA, SF  
793 and VO). The second column lists the percentage of variance explained (PVE) by each  
794 EOF, the following columns describe the spatial patterns.

795

796 Table 6. SVD analysis of the variable pair GPS height (a) and precipitation residuals (b).  
797 Five GPS stations (MSEL, MEDI, RA, BOLG and BR) and four precipitation stations  
798 (ME, RA, BO and BR). The two stations at Medicina, MSEL and MEDI, are coupled to  
799 the same ME precipitation data series. The second column lists the squared covariance  
800 percentage relevant to each SVD, the following columns describe the spatial patterns.

801

802 Table 7. SVD analysis of the variable pair GPS height (a) and precipitation residuals (b).  
803 Eight GPS stations (MSEL, MEDI, RA, BOLG, BR, CA, SF and VO) and seven  
804 precipitation stations (ME, RA, BO, BR, CA, SF and VO). The two stations at Medicina,  
805 MSEL and MEDI, are coupled to the same ME precipitation data series. The second  
806 column lists the squared covariance percentage relevant to each SVD, the following  
807 columns describe the spatial patterns.

808

809 Table 8. EOF analysis of two time series, GPS height and water table residuals, at  
810 Medicina. The second column lists the percentage of variance explained (PVE) by each  
811 EOF, the following columns describe the spatial patterns. (a) MSEL and water table; (b)  
812 MEDI and water table.

813

814 Table 9. EOF analysis of two time series, superconducting gravimeter (SG) and local  
815 hydrology residuals, at Medicina. The second column lists the percentage of variance  
816 explained (PVE) by each EOF, the following columns describe the spatial patterns. (a)  
817 SG and precipitation; (b) SG and water table.

818

819 Table 10. EOF analysis of two time series, GPS height and superconducting gravimeter  
820 (SG) residuals, at Medicina. The second column lists the percentage of variance  
821 explained (PVE) by each EOF, the following columns describe the spatial patterns. (a)  
822 MEDI and SG; (b) MSEL and SG.

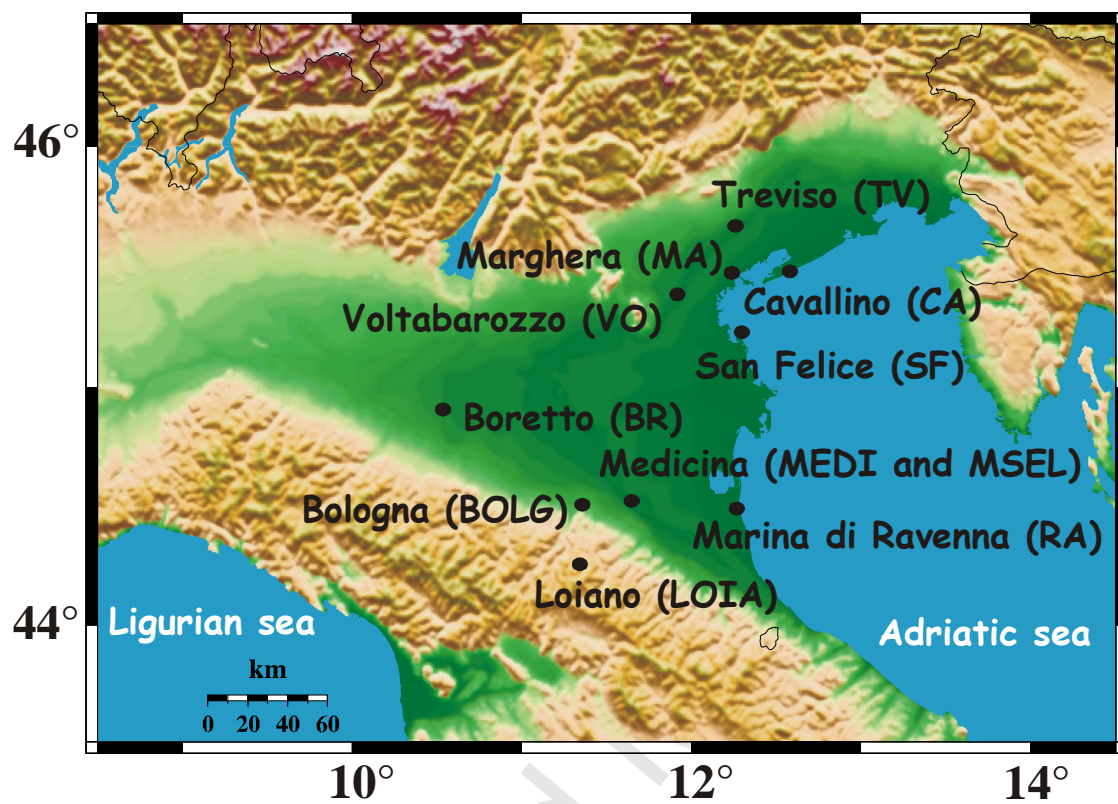


Figure 1



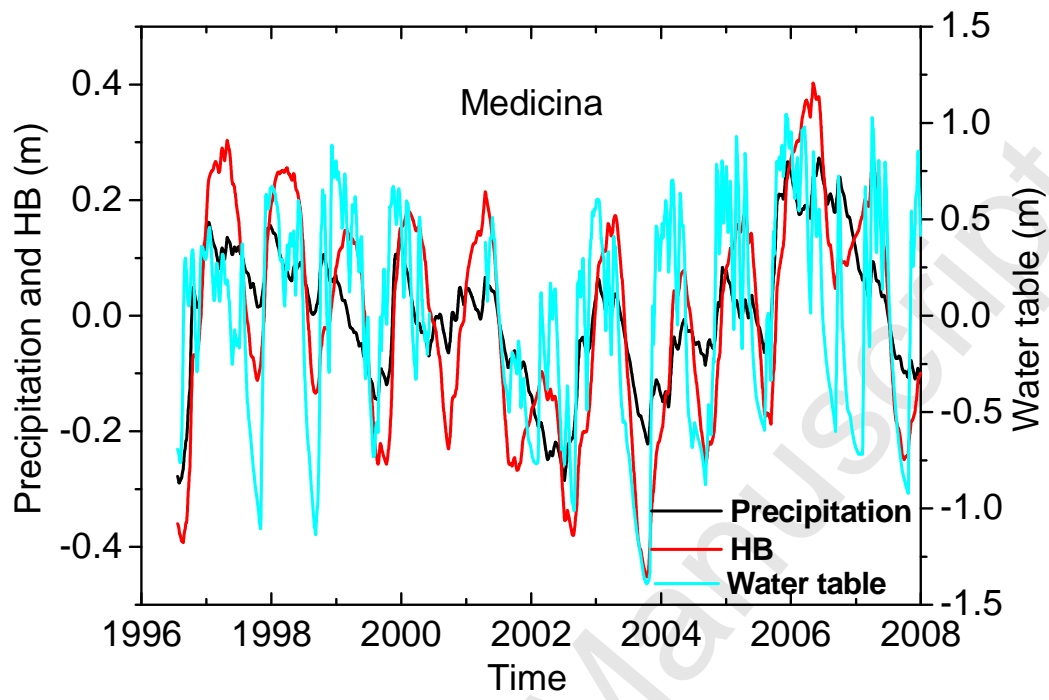


Figure 2

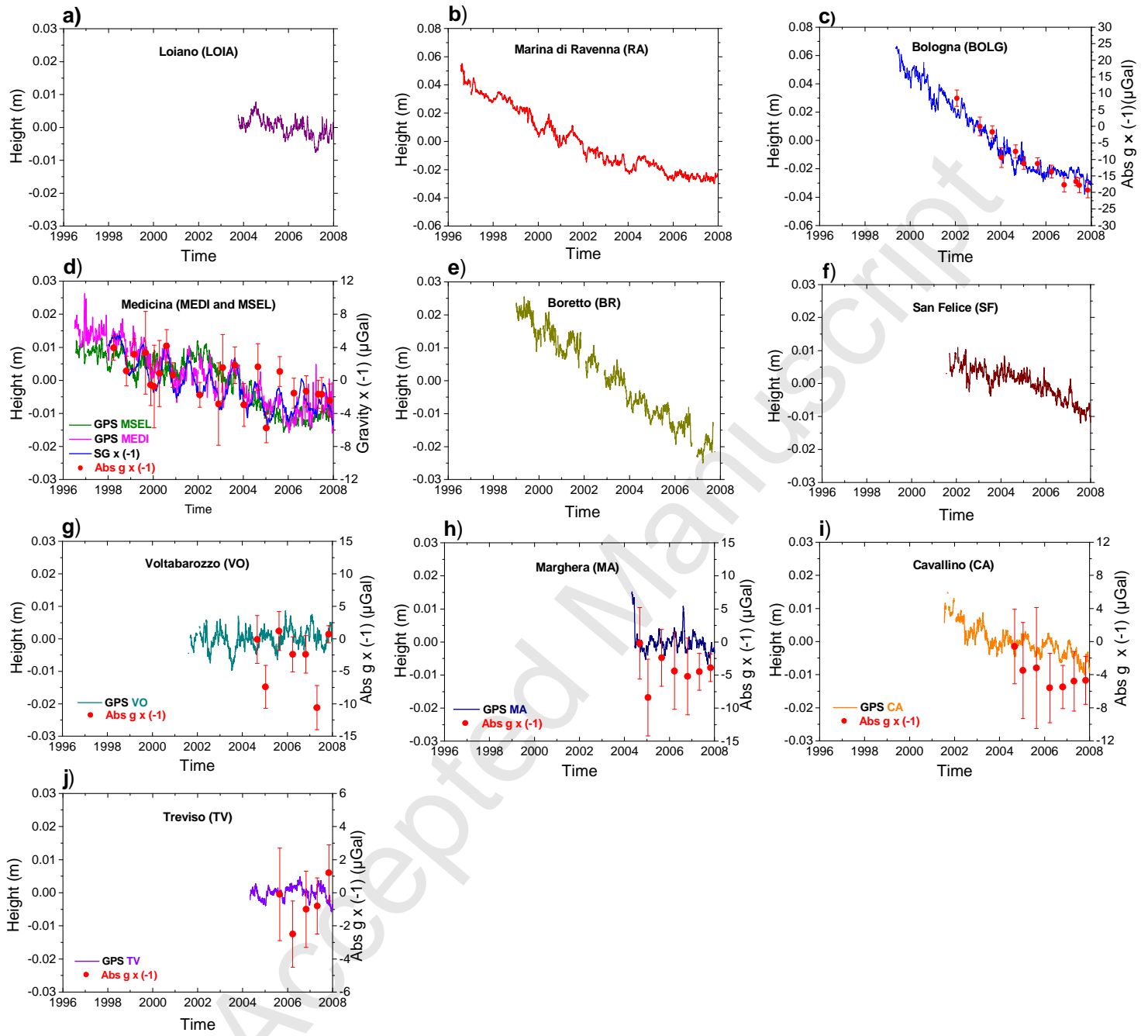


Figure 3

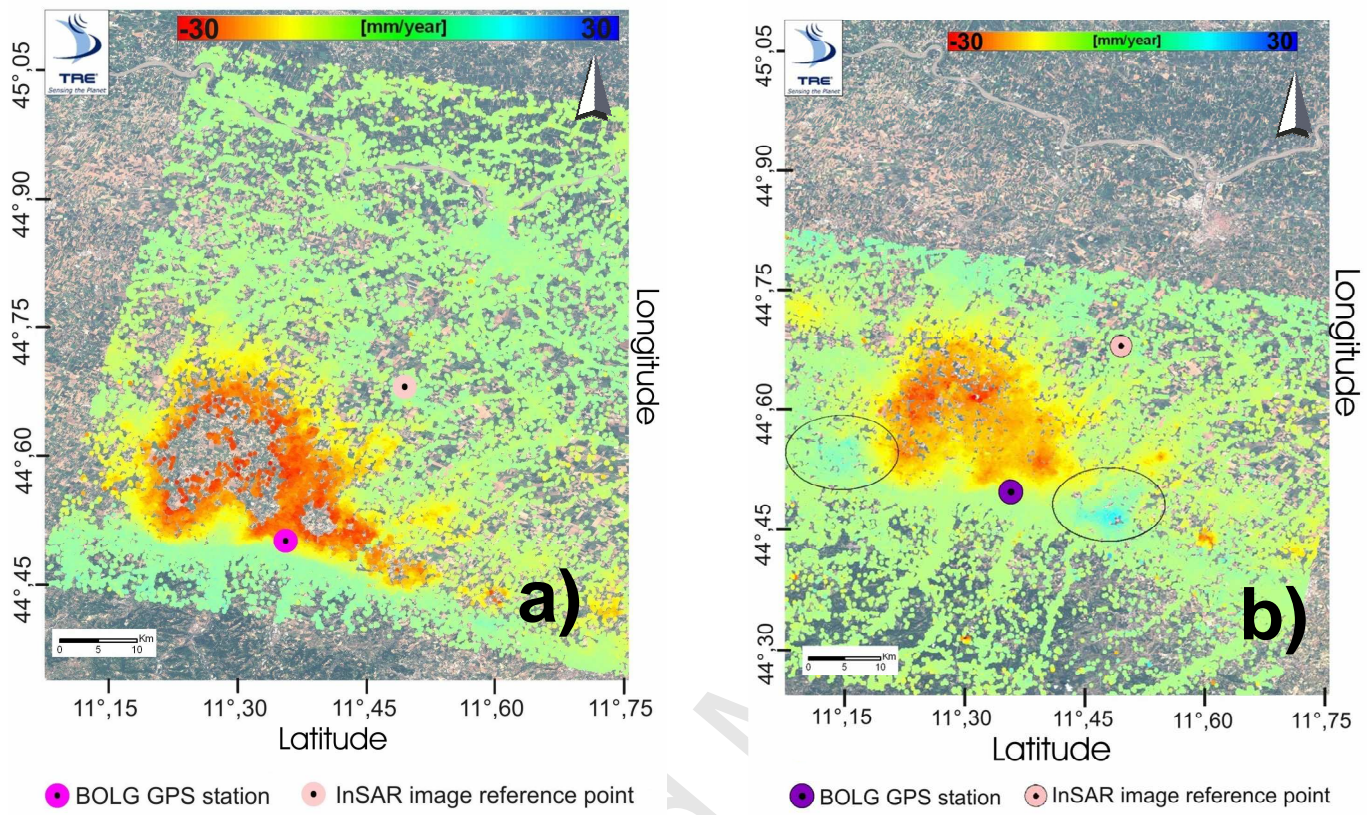


Figure 4

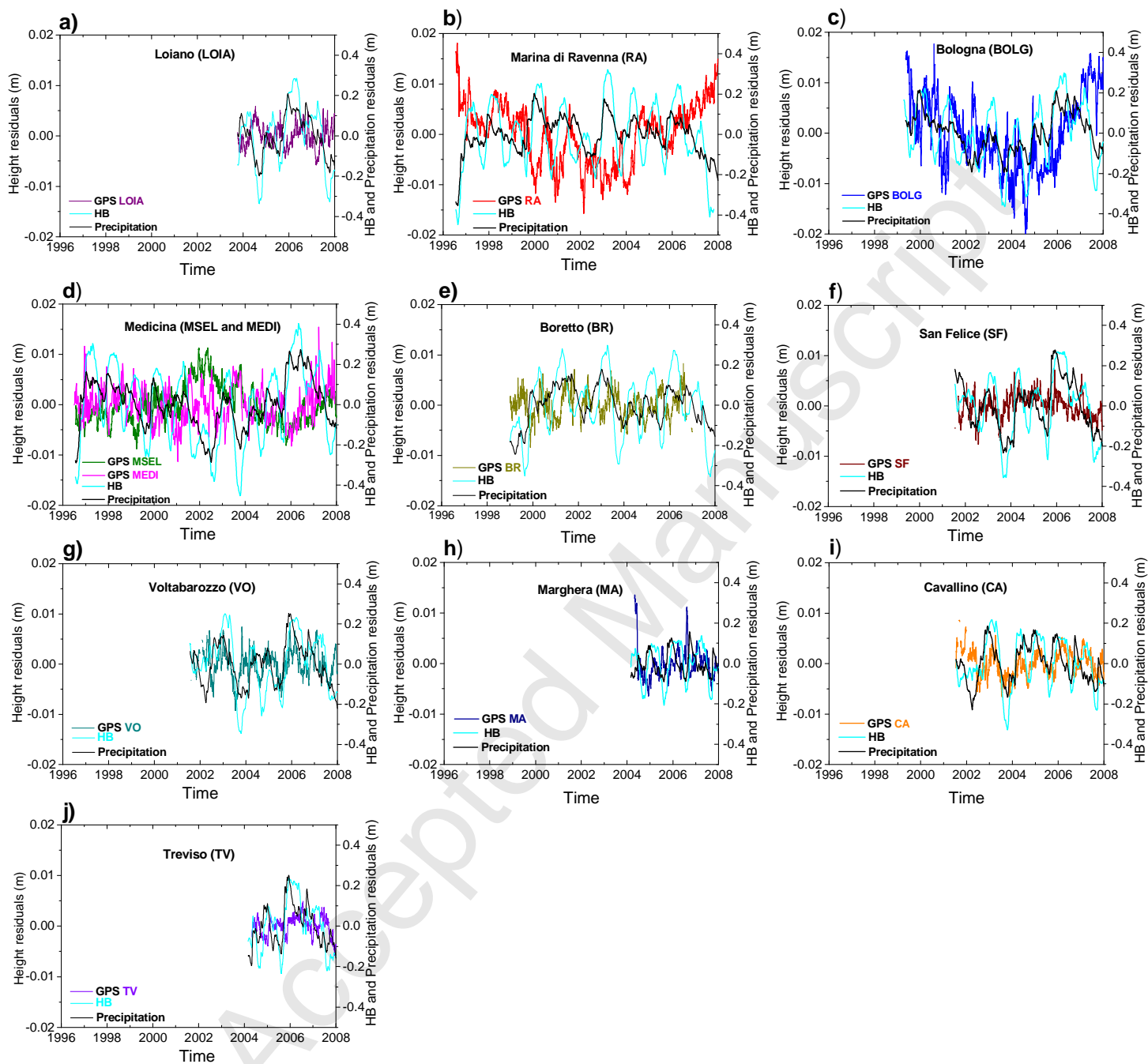


Figure 5

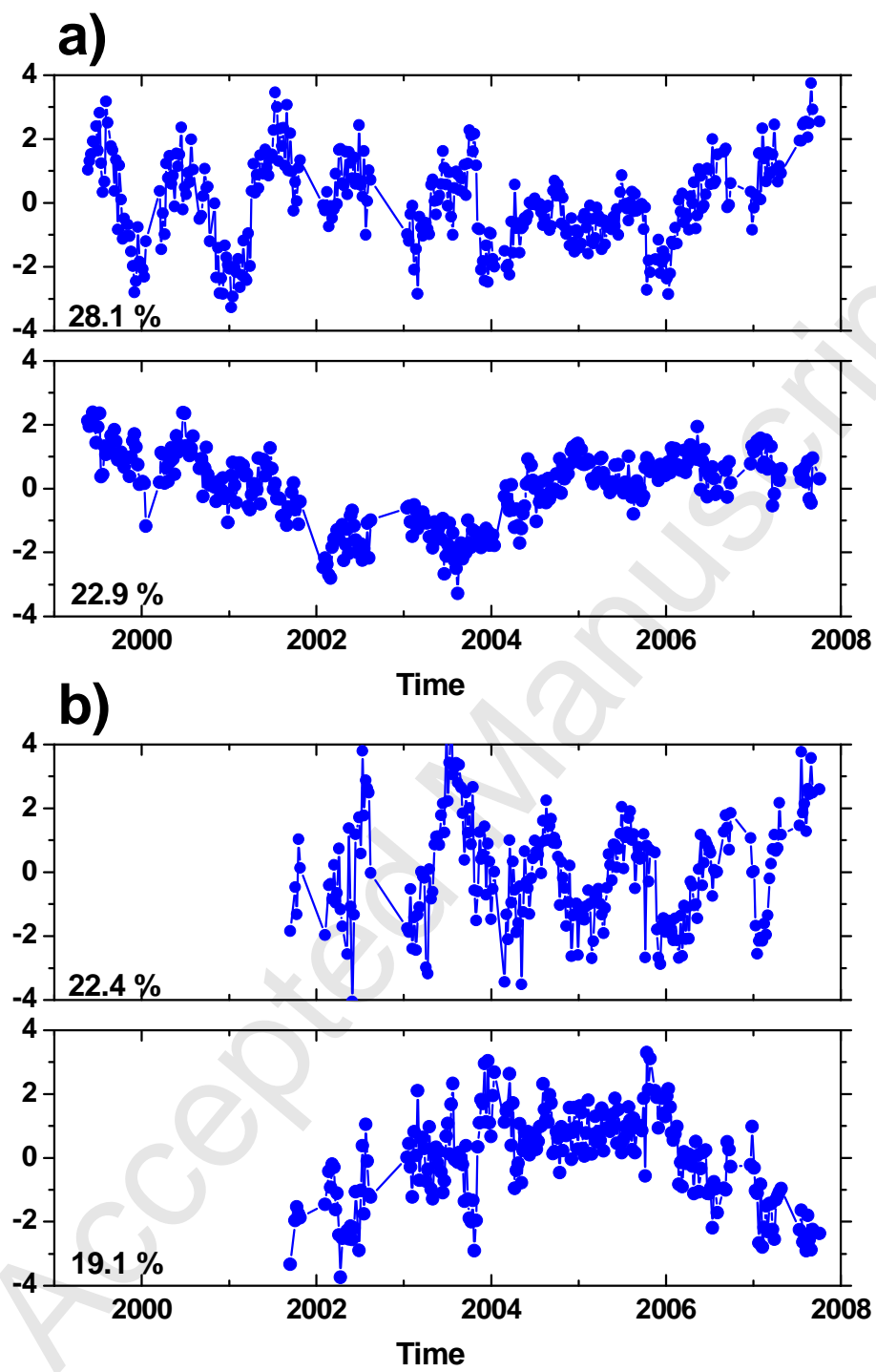


Figure 6

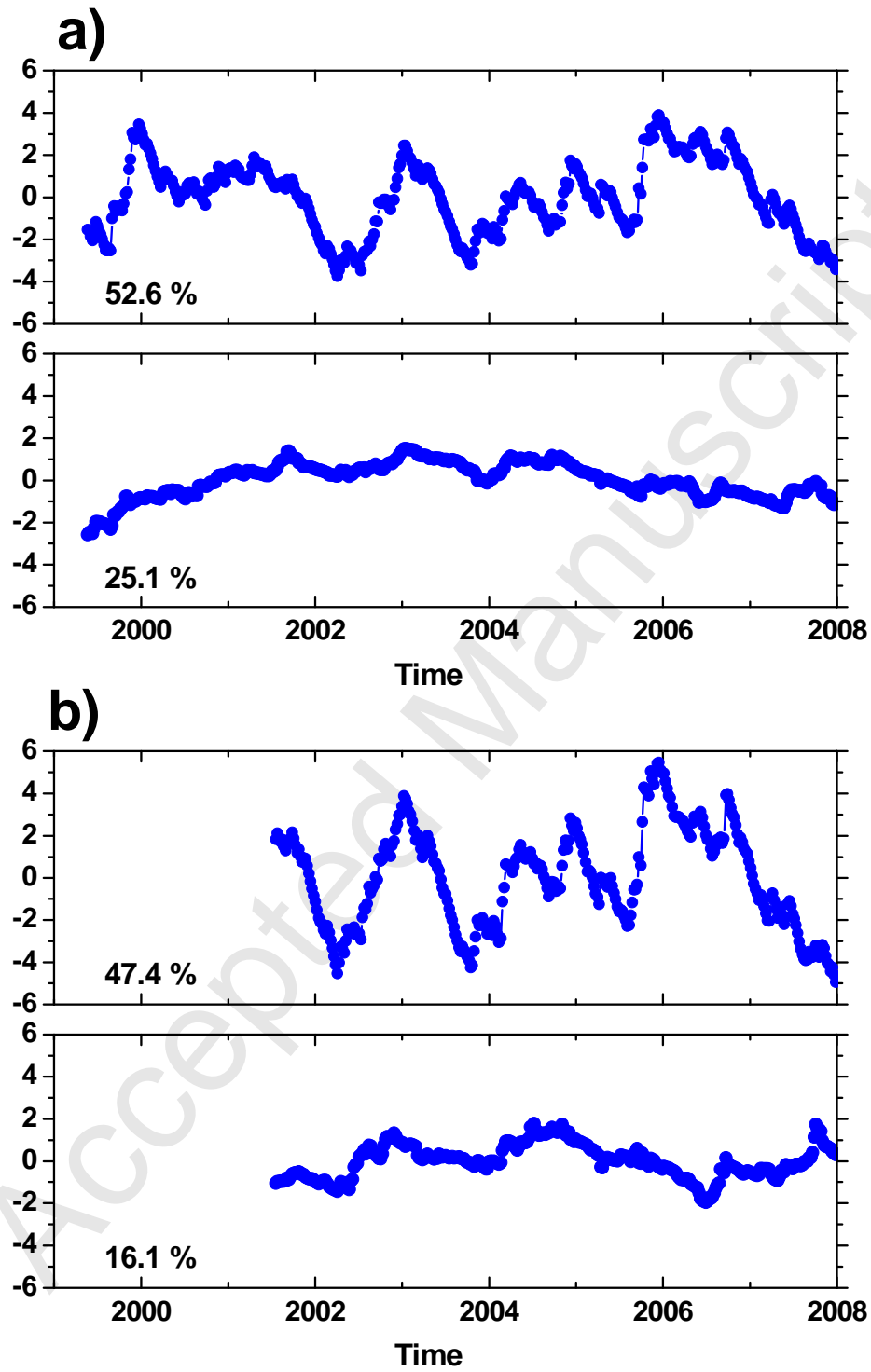


Figure 7

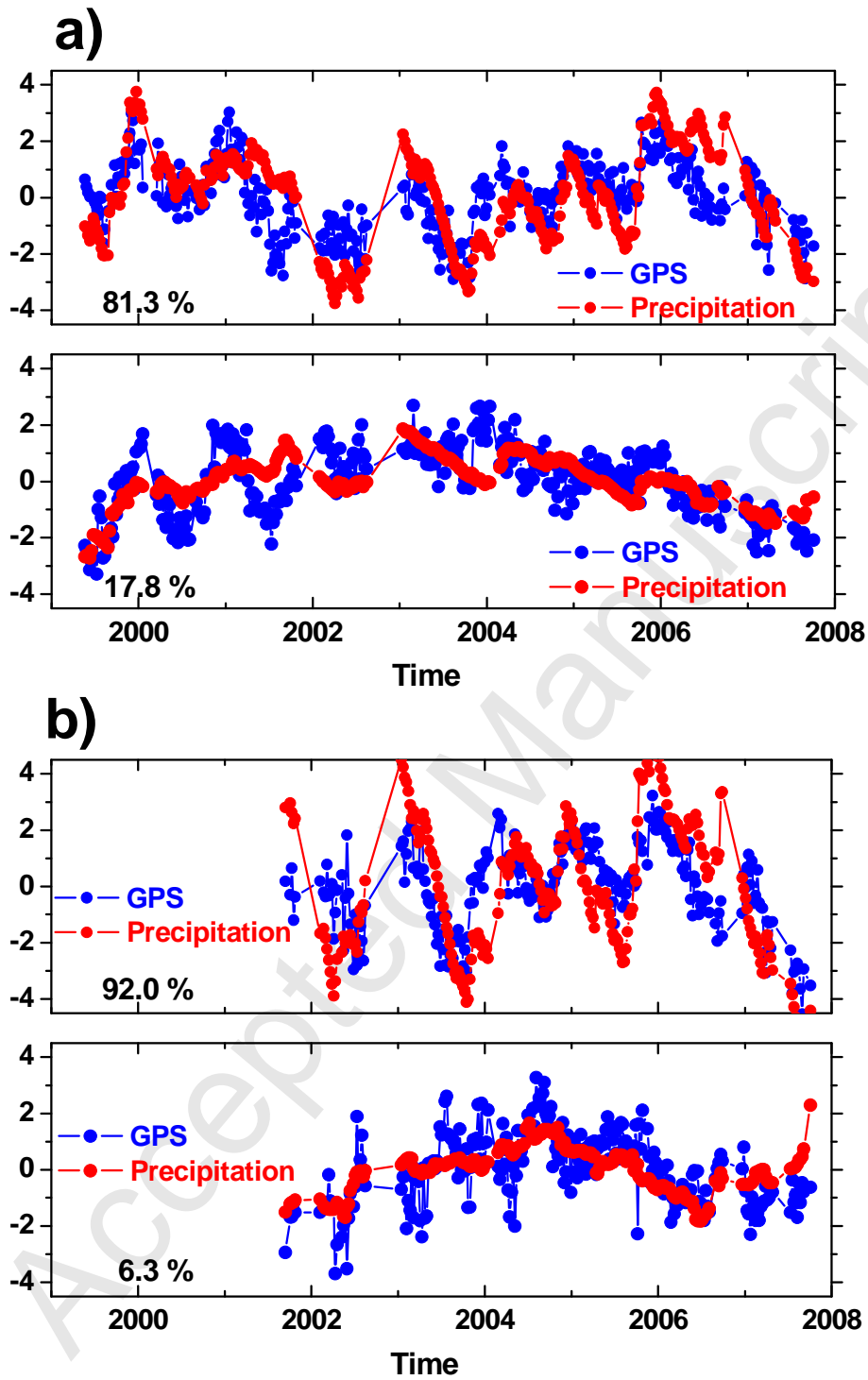


Figure 8

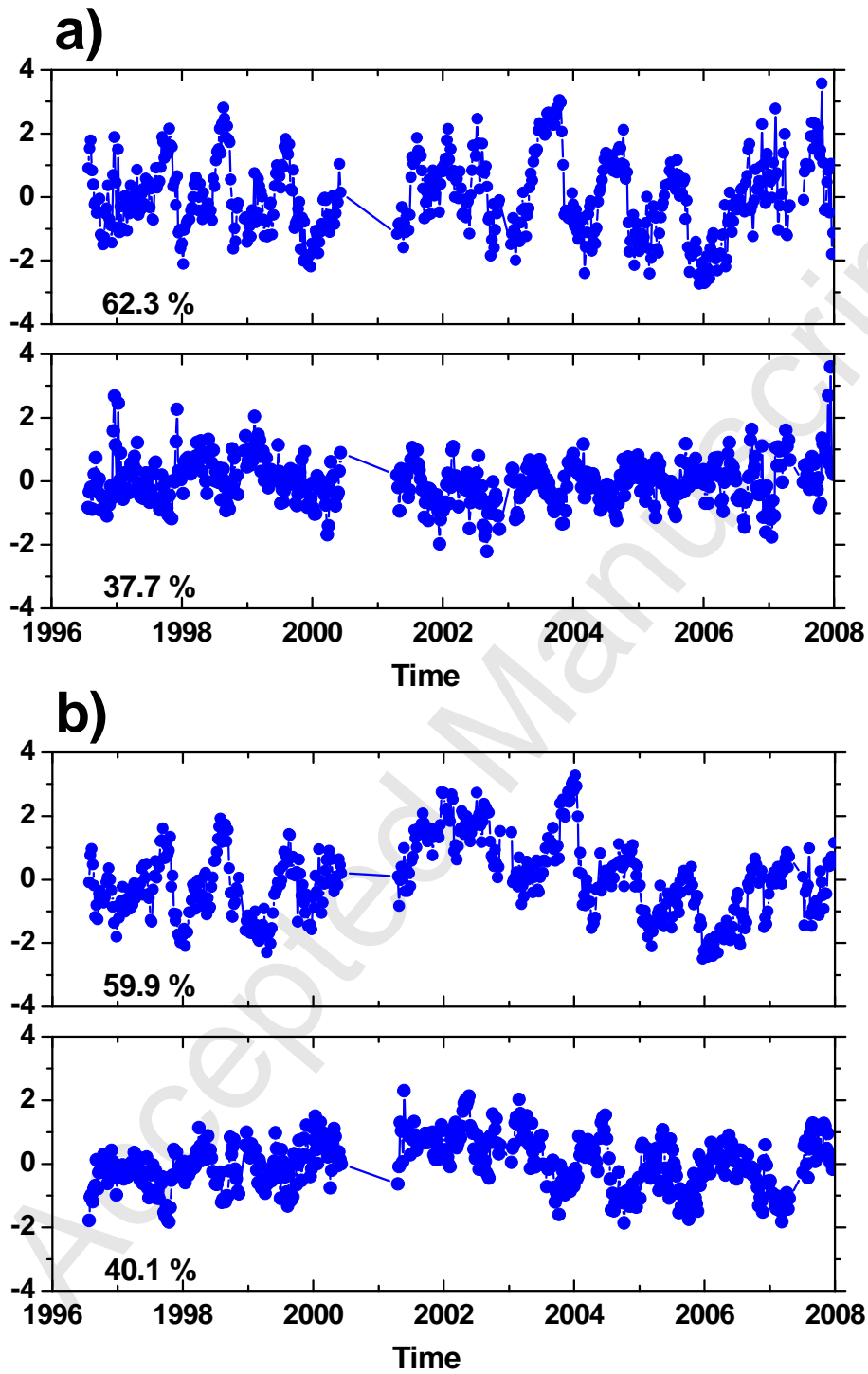


Figure 9



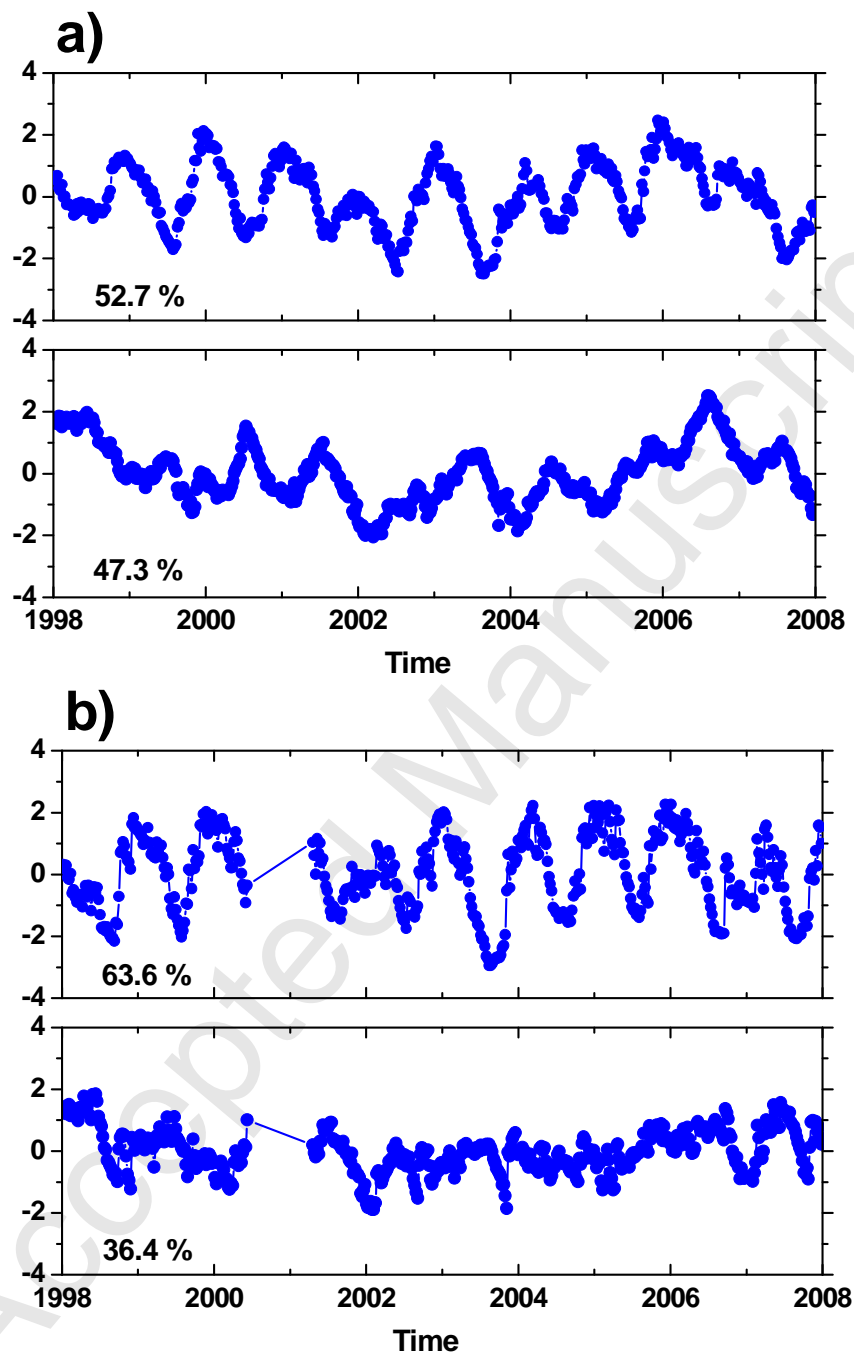


Figure 10

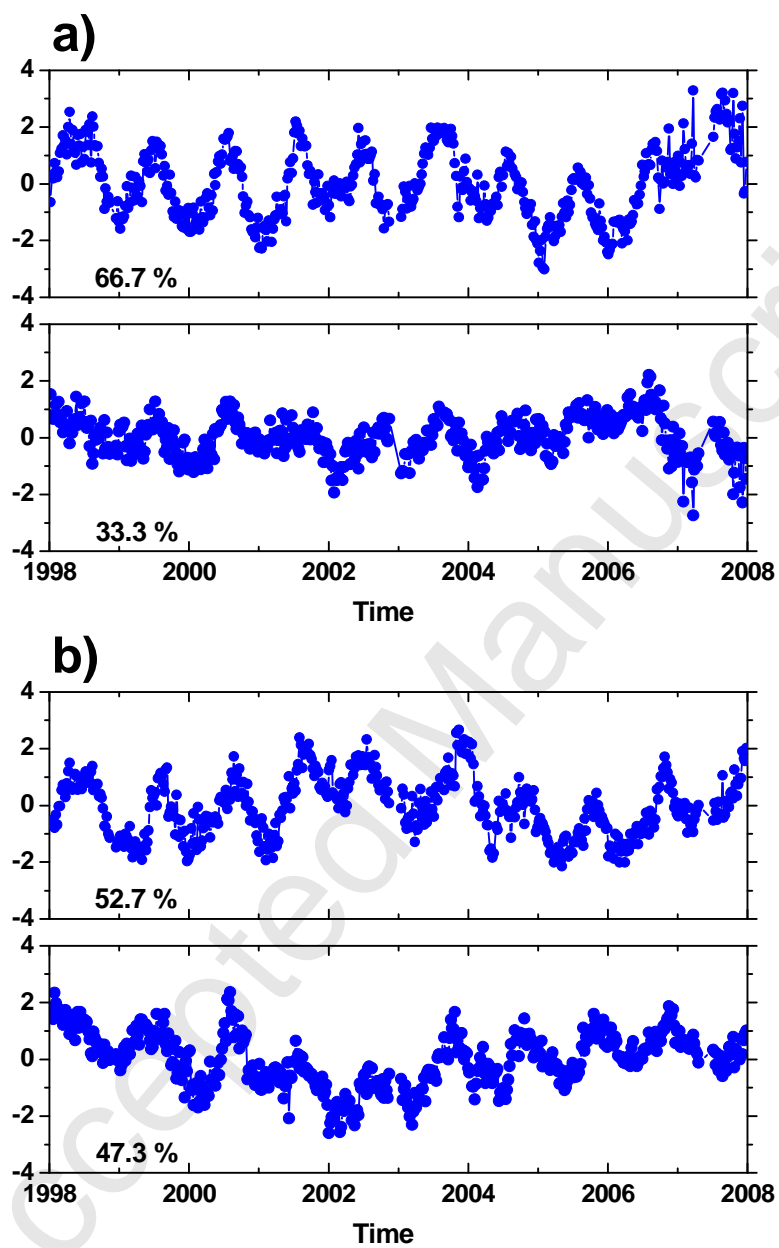


Figure 11

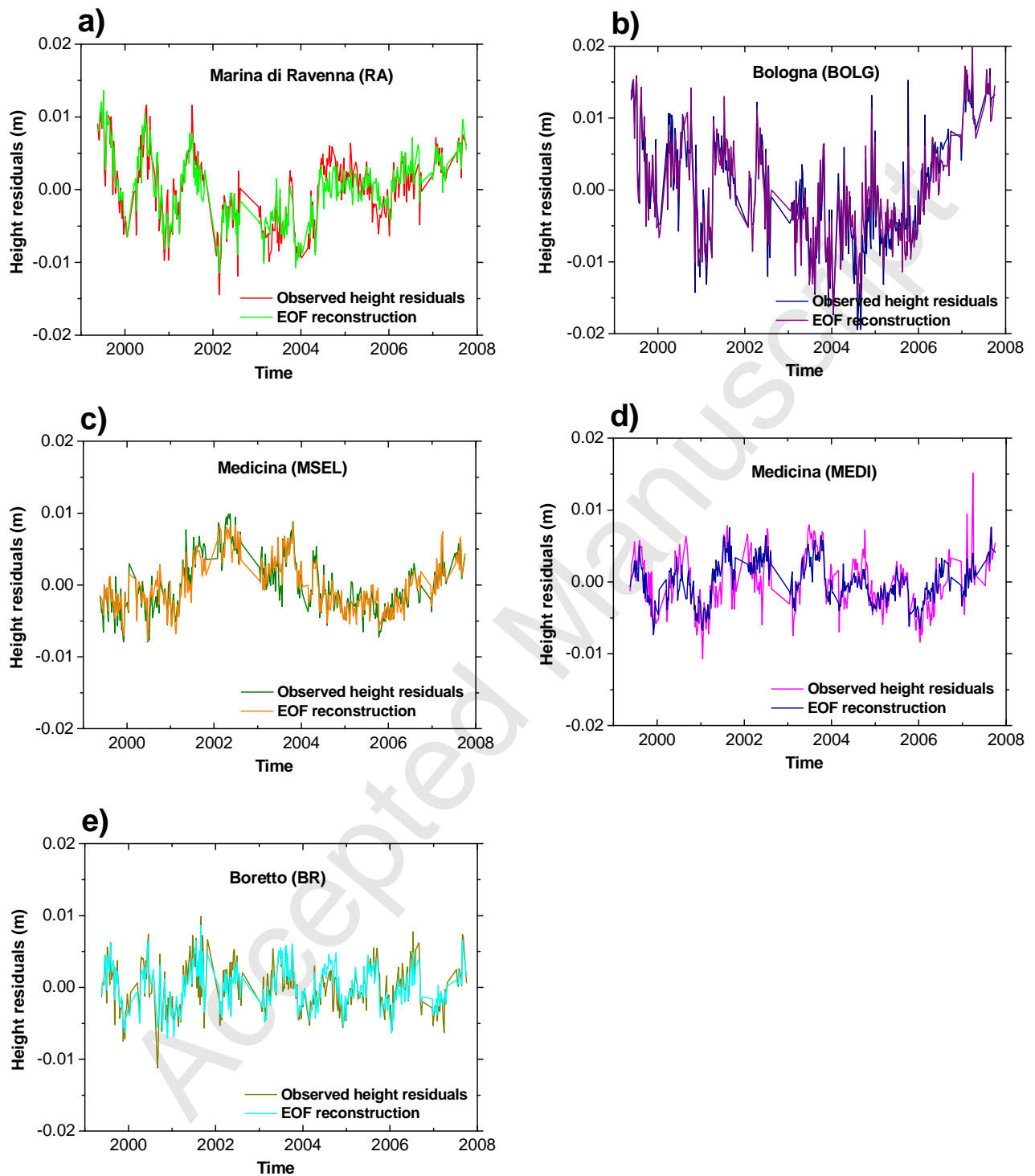


Figure 12

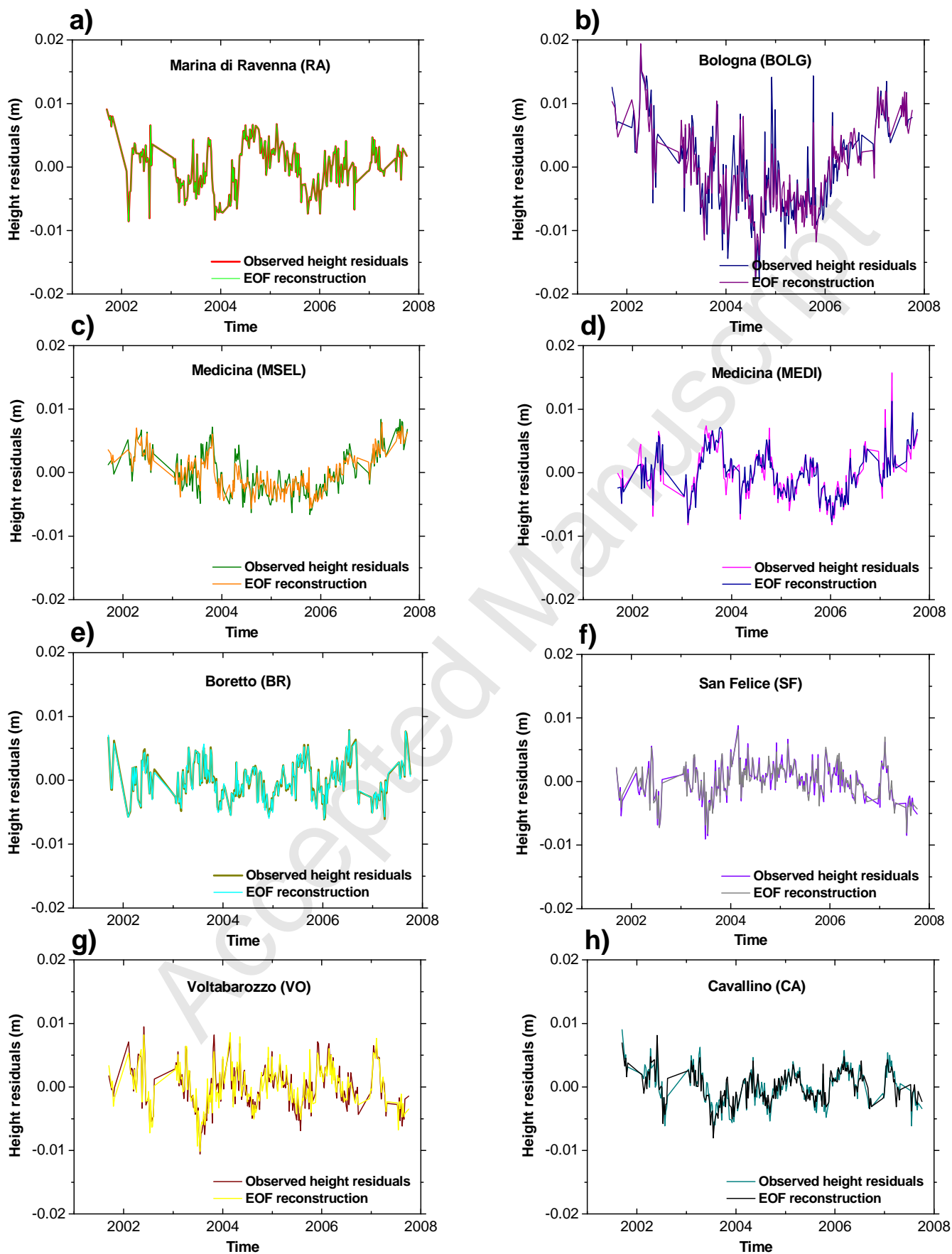


Figure 13

Table 1.

Station name	North/South	Technique	Linear trend
			(mm/yr) GPS ( $\mu$ Gal/yr) SG, AG
Loiano <sup>(a)</sup> (LOIA)	S	GPS	-1.41 $\pm$ 0.25
		AG	-----
Marina di Ravenna (RA)	S	GPS	-6.51 $\pm$ 0.15
Bologna (BOLG)	S	GPS	-10.57 $\pm$ 0.25
		AG	+4.17 $\pm$ 1.75
		SG	+0.71 $\pm$ 0.05
Medicina (Gravity)	S	AG	+0.52 $\pm$ 0.65
		GPS	-2.44 $\pm$ 0.25
Medicina <sup>(b)</sup> (MEDI)	S	GPS	-2.44 $\pm$ 0.25
Medicina (MSEL)	S	GPS	-2.13 $\pm$ 0.10
Boretto (BR)	S	GPS	-5.00 $\pm$ 0.10
San Felice (SF)	N	GPS	-2.24 $\pm$ 0.15
		GPS	+0.36 $\pm$ 0.15
Votabarozzo (VO)	N	AG	-0.98 $\pm$ 1.07
		GPS	-0.88 $\pm$ 0.40
Marghera (MA)	N	AG	-0.88 $\pm$ 1.41
		GPS	-1.97 $\pm$ 0.15
Cavallino (CA)	N	AG	+0.29 $\pm$ 1.46
		GPS	0.00 $\pm$ 0.25
Treviso (TV)	N	AG	-1.64 $\pm$ 1.50

Table 10

(a)

EOF	PVE	MEDI	SG
1	66.7	+0.71	-0.71
2	33.3	-0.71	-0.71

(b)

EOF	PVE	MSEL	SG
1	52.7	+0.71	-0.71
2	47.3	-0.71	-0.71

Accepted Manuscript

Table 2

EOF	PVE	GPS spatial pattern				
		MSEL	MEDI	RA	BOLG	BR
1	28.1	+0.38	+0.50	+0.43	+0.44	+0.47
2	22.9	-0.62	-0.29	+0.62	+0.37	-0.10
3	19.2	+0.36	-0.08	-0.17	+0.64	-0.65
4	17.1	-0.25	+0.76	+0.16	-0.25	-0.52
5	12.6	-0.53	+0.29	-0.61	+0.44	+0.27

Accepted Manuscript

Table 3

EOF	PVE	GPS spatial pattern							
		MSEL	MEDI	RA	BOLG	BR	CA	SF	VO
1	22.4	+0.12	+0.41	+0.03	-0.13	+0.22	-0.47	-0.48	-0.54
2	19.1	-0.60	-0.26	-0.26	-0.59	-0.24	-0.26	+0.07	-0.13
3	14.5	+0.22	+0.08	-0.70	+0.30	-0.53	-0.19	-0.18	+0.10
4	11.8	+0.01	+0.14	+0.62	-0.01	-0.76	-0.08	-0.07	-0.03
5	11.1	-0.05	-0.66	+0.06	+0.20	-0.03	+0.26	-0.62	-0.25
6	8.2	-0.66	+0.50	-0.09	+0.31	-0.02	+0.42	-0.18	-0.07
7	6.9	+0.36	+0.20	-0.18	-0.57	-0.15	+0.64	-0.10	-0.18
8	5.9	-0.04	+0.12	+0.07	-0.27	+0.11	-0.09	-0.55	+0.76



Table 4

EOF	PVE	Precipitation spatial pattern			
		ME	RA	BO	BR
1	52.6	+0.55	+0.50	+0.49	+0.46
2	25.1	-0.29	+0.38	-0.63	+0.61
3	15.9	+0.07	-0.77	+0.11	+0.62
4	6.5	-0.78	+0.14	+0.59	+0.15

Accepted Manuscript

Table 5

EOF	PVE	Precipitation spatial pattern						
		ME	RA	BO	BR	CA	SF	VO
1	47.4	+0.40	+0.36	+0.37	+0.41	+0.32	+0.39	+0.39
2	16.1	-0.30	+0.09	-0.50	+0.03	+0.78	-0.13	+0.16
3	13.1	+0.21	+0.79	-0.04	-0.10	0.00	-0.35	-0.45
4	7.6	-0.07	+0.33	-0.45	-0.41	-0.26	+0.65	+0.18
5	6.3	0.00	-0.19	+0.14	-0.02	+0.35	+0.52	-0.74
6	5.8	-0.05	+0.01	+0.52	-0.78	+0.29	-0.08	+0.19
7	3.7	+0.84	-0.31	-0.35	-0.23	+0.12	-0.10	+0.01

Table 6

(a)

SVD	SCP	GPS spatial pattern				
		MSEL	MEDI	RA	BOLG	BR
1	81.3	-0.64	-0.72	-0.01	+0.05	-0.27
2	17.8	+0.24	-0.21	-0.59	-0.73	-0.11
3	0.8	-0.72	+0.52	-0.05	-0.38	+0.24
4	0.0	-0.13	+0.31	-0.68	+0.48	-0.43

(b)

SVD	SCP	Precipitation spatial pattern			
		ME	RA	BO	BR
1	81.3	+0.59	+0.46	+0.56	+0.36
2	17.8	-0.26	+0.64	-0.56	+0.47
3	0.8	+0.23	+0.53	-0.17	-0.80
4	0.0	-0.73	+0.32	+0.59	-0.13

Table 7

(a)

SVD	SCP	GPS spatial pattern							
		MSEL	MEDI	RA	BOLG	BR	CA	SF	VO
1	92.0	-0.55	-0.59	-0.13	-0.19	-0.20	+0.34	+0.25	+0.28
2	6.3	-0.36	+0.23	+0.20	-0.62	-0.19	-0.52	+0.19	-0.23
3	1.3	+0.03	+0.05	-0.95	-0.18	+0.16	-0.16	+0.02	-0.08
4	0.2	+0.03	-0.36	-0.08	+0.40	-0.45	-0.67	-0.16	+0.16
5	0.1	-0.64	+0.17	-0.07	+0.35	-0.02	+0.11	-0.45	-0.46
6	0.1	+0.20	+0.27	-0.15	+0.09	-0.77	+0.32	+0.29	-0.26
7	0.0	+0.25	-0.59	+0.07	-0.04	+0.14	-0.02	+0.14	-0.74

(b)

SVD	SCP	Precipitation spatial pattern						
		ME	RA	BO	BR	CA	SF	VO
1	92.0	+0.39	+0.39	+0.38	+0.37	+0.39	+0.39	+0.33
2	6.3	-0.22	+0.24	-0.50	-0.19	+0.76	-0.16	+0.06
3	1.3	+0.24	+0.58	+0.29	-0.45	-0.15	-0.54	+0.01
4	0.2	-0.46	-0.35	+0.54	-0.23	+0.21	-0.14	+0.51
5	0.1	+0.45	-0.36	-0.16	+0.39	+0.09	-0.63	+0.29
6	0.1	-0.13	-0.06	+0.44	+0.30	+0.35	-0.27	-0.71
7	0.0	-0.56	+0.43	-0.09	+0.57	-0.28	-0.22	+0.20

Table 8

(a)

EOF	PVE	MEDI	WT
1	62.3	+0.71	-0.71
2	37.7	+0.71	+0.71

(b)

EOF	PVE	MSEL	WT
1	59.9	+0.71	-0.71
2	40.1	+0.71	+0.71

Accepted Manuscript

Table 9

(a)

EOF	PVE	Prec.	SG
1	52.7	+0.71	+0.71
2	47.3	+0.71	-0.71

(b)

EOF	PVE	WT	SG
1	63.6	+0.71	+0.71
2	36.4	+0.71	-0.71

Accepted Manuscript